The M1 aminopeptidase NPEPPS is a novel regulator of cisplatin sensitivity

Robert T. Jones[1,15], Andrew Goodspeed[1,3,15], Maryam C. Akbarzadeh[2,4,16], Mathijs Scholtes[2,16], Hedvig Vekony[1], Annie Jean[1], Charlene B. Tilton[1], Michael V. Orman[1], Molishree Joshi[1,5], Teemu D. Laajala[1,6], Mahmood Javaid[7], Eric T. Clambey[8], Ryan Layer[7,9], Sarah Parker[10], Tokameh Mahmoudi[2,11], Tahlita Zuiverloon[2,*], Dan Theodorescu[12,13,14,*], James C. Costello[1,3,*]

[1]Department of Pharmacology, University of Colorado Anschutz Medical Campus, Aurora, CO, USA
[2] Department of Urology, Erasmus MC Cancer Institute, Erasmus University Medical Center Rotterdam, Rotterdam, The Netherlands
[3]University of Colorado Comprehensive Cancer Center, University of Colorado Anschutz Medical Campus, Aurora, CO, USA
[4]Stem Cell and Regenerative Medicine Center of Excellence, Tehran University of Medical Sciences, Tehran, Iran
[5]Functional Genomics Facility, University of Colorado Anschutz Medical Campus, Aurora, CO, USA
[6]Department of Mathematics and Statistics, University of Turku, Turku, Finland.
[7]Computer Science Department, University of Colorado, Boulder
[8]Department of Anesthesiology, University of Colorado Anschutz Medical Campus, Aurora, CO
[9]BioFrontiers Institute, University of Colorado, Boulder
[10]Heart Institute & Advanced Clinical Biosystems Research Institute, Cedars Sinai Medical Center, Los Angeles, California 90048, United States
[11]Erasmus MC, Department of Biochemistry, Rotterdam, The Netherlands
[12]Department of Surgery, Cedars-Sinai Medical Center, Los Angeles, CA, USA
[13]Department of Pathology and Laboratory Medicine, Cedars-Sinai Medical Center, Los Angeles, CA, USA
[14]Cedars-Sinai Samuel Oschin Comprehensive Cancer Institute, Los Angeles, CA, USA
[15]These authors contributed equally
[16]These authors contributed equally
*Corresponding Authors

Corresponding Authors
Tahlita Zuiverloon, MD, PhD
Department of Urology
Erasmus MC Cancer Institute, Erasmus University Medical Center
Dr. Molewaterplein 40
3015GD, Rotterdam
The Netherlands
+31 6 26 41 90 87
t.zuiverloon@erasmusmc.nl

Dan Theodorescu, MD, PhD
Department of Surgery and Pathology
Cedars-Sinai Medical Center
8700 Beverly Blvd.
OCC Mezz C2002
Los Angeles, CA 90048

+1 (310) 423-8431
dan.theodorescu@cshs.org

James C Costello, PhD
Department of Pharmacology
University of Colorado Anschutz Medical Campus
Mail Stop 8303
12801 E. 17th Ave., Rm L18-6114
Aurora, CO 80045
+1 (303) 724-8619
james.costello@cuanschutz.edu

HIGHLIGHTS

- CRISPR screens with multi-omics identify NPEPPS as a driver of cisplatin resistance
- NPEPPS depletion in multiple bladder cancer models enhances cisplatin sensitivity
- LRRC8A and LRRC8D loss increase resistance to cisplatin in CRISPR screens
- Unique resource of functional and multi-omic data is provided to the community

KEY WORDS

Bladder Cancer, CRISPR Screen, Synthetic Lethality, Genomics, Transcriptomics, Proteomics, DNA Repair, Cisplatin, Chemotherapy, NPEPPS, Volume Regulated Anion Channel, VRAC, LRRC8A, LRRC8D, Tosedostat

ABSTRACT

Platinum-based chemotherapeutics are used in many combination regimens in cancer. Despite extensive use across diverse cancer types, there is room for improved efficacy and patient selection for treatment. Here, we use bladder cancer to address both issues. A multi-omic assessment of five human bladder cancer cell lines and their chemotherapy resistant derivatives, coupled with *in vitro* whole-genome CRISPR screens were used to define functional drivers of treatment resistance. We identified 46 genes that sensitized the resistant cell lines to cisplatin plus gemcitabine (GemCis), a standard combination therapy in bladder cancer. Most genes were involved with DNA damage and repair pathways, which have previously been associated with enhanced sensitivity to cisplatin. Evaluating expression of the 46 genes in the whole transcriptome and proteome data in parental and resistant lines identified the puromycin sensitive aminopeptidase, NPEPPS, as a novel hit. Depletion of NPEPPS resulted in sensitizing resistant bladder cancer cells to cisplatin *in vitro* and in xenograft experiments. Pharmacologic inhibition of NPEPPS with tosedostat in cells and in chemoresistant, bladder cancer patient tumor-derived organoids improved response to cisplatin. Prior work found NPEPPS in a protein complex with volume regulated anion channels (VRACs) in several cell line models. Interestingly, depletion of two VRAC subunits, LRRC8A and LRRC8D, known importers of intracellular cisplatin, enhanced resistance to cisplatin. Our findings support NPEPPS as a novel and druggable driver of cisplatin resistance with the potential for rapid translation to clinical investigation.

INTRODUCTION

Platinum-based chemotherapeutics have a long history (Dilruba and Kalayda, 2016) with successful applications in testicular, ovarian, bladder, head and neck, and lung cancers. However, these drugs come with dose-dependent side effects that limit patient eligibility. Additionally, chemoresistance mechanisms can arise, reducing the efficacy of these drugs. While mechanisms of resistance have long been established, including DNA damage repair and drug export (Galluzzi et al., 2012), other mechanisms, such as the import of platinum drugs through volume regulated anion channels (VRACs) are more recently discovered and present new opportunities for therapeutic development (Planells-Cases et al., 2015a; Rottenberg et al., 2021). Despite their limitations, platinum-based drugs remain the standard of care in many cancer types and with a paucity of better treatment options for many patients, these drugs will remain in use for the foreseeable future. Two avenues can be taken to improve patient outcomes, which include discovery of more effective agents or development of strategies that can improve efficacy of platinum-based regimens. The latter would have broad impact across a range of cancer types. Here we focus on the latter approach and use bladder cancer as the model.

Bladder cancer (BCa) accounts for 430,000 new diagnoses and 170,000 deaths worldwide annually (Bray et al., 2018). Cisplatin-based combination chemotherapy, in the form of gemcitabine plus cisplatin (GemCis) or Methotrexate, Vinblastine, Adriamycin, and Cisplatin (MVAC), remains the first-line, standard of care for metastatic BCa, providing a 5-10% cure rate. However, up to 30% of patients are ineligible for cisplatin-based treatment (Galsky et al., 2018) and are offered carboplatin-based combinations. Unfortunately carboplatin combination therapy has been shown to be less effective in BCa (Patel et al., 2020). Alternatively, immune checkpoint therapies (ICT) are being considered as a first-line therapy (Galsky et al., 2020); however, ICT requires a PD-L1 diagnostic test, for which only ~25% patients meet eligibility (Nadal and Bellmunt, 2019). The complete response rates for ICT eligible patients is 20-30% (Balar et al., 2017a, 2017b). Cisplatin-based combination chemotherapy is also standard of care in the neoadjuvant (NAC) setting for the management of localized muscle-invasive bladder cancer (Grossman et al., 2003; Vale, 2005). However, NAC adoption has been relatively slow due to the toxicity of the drugs, the number of patients that are cisplatin ineligible, and the relatively small survival benefit of 5-15% over immediate cystectomy (Witjes et al., 2020). Importantly, in both the metastatic and NAC BCa settings, patient selection and therapeutic efficacy of cisplatin-based chemotherapy are critical unresolved challenges (Patel et al., 2020).

Recently, several large-scale efforts have performed whole genome loss-of-function screening across hundreds of cancer cell lines using CRISPR- and shRNA-based libraries to define pan-cancer and context-specific genetic dependencies (Cowley et al., 2014; McDonald et al., 2017; Tsherniak et al., 2017; Behan et al., 2019). A limitation of these efforts in pharmacogenomics is that cells were grown under basal growth conditions in the absence of treatment. Additionally, those studies were performed in cell lines that had not acquired resistance to the treatment. To better understand the functional drivers of therapeutic resistance, such screens must be done in the presence and absence of the therapy of interest (Goodspeed et al., 2019; Huang et al., 2020; Jost and Weissman, 2018; Olivieri et al., 2020), and in cells that have acquired resistance to the treatment itself. Results from such synthetic lethal screens can be used to prioritize gene candidates that can be targeted to overcome treatment resistance.

In this study, we harnessed the power of CRISPR-based synthetic lethal screening and multi-omic profiling to systematically assess the functional determinants of sensitivity to the treatment regimen of gemcitabine plus cisplatin in a panel of chemoresistant BCa cell lines (**Figure 1A**). In

addition to known mechanisms, we present the finding that upregulation of puromycin-sensitive aminopeptidase, NPEPPS, is a novel mechanism of gemcitabine plus cisplatin resistance, specifically affecting cisplatin sensitivity. We provide validations of these findings *in vitro* and *in vivo*. We next show that pharmacological inhibition of NPEPPS through an orally deliverable, well-tolerated drug, tosedostat, re-sensitizes resistant cells to cisplatin treatment in BCa cell lines and organoids derived from patient tumors that did not response to cisplatin-based chemotherapy .We also provide a unique resource to the community, an R Shiny app for broad comparisons between datasets (CRISPR screens and multi-omic) and cell lines, along with individual gene queries and basic plotting functionality (https://bioinformatics.cuanschutz.edu/GC_Visualization/).

RESULTS

From the Resistant Cancer Cell Line (RCCL) collection (Vallo et al., 2015, 2017), we obtained five human BCa cell lines, KU1919, 5637, T24, TCCSUP, and 253J. For each, we obtained the parental lines (-Par) and their matched derivatives that were made resistant through dose escalation to cisplatin (-Cis), gemcitabine (-Gem), and gemcitabine plus cisplatin (-GemCis) concurrently (**Figure 1A; Table S1**). We confirmed resistance to the associated drugs for all resistant derivatives in comparison to the parental lines and found them to be consistent with those reported by RCCL (**Figure S1**) (Vallo et al., 2015, 2017). These cells represent features and alterations in putative BCa drivers as reported in TCGA (Robertson et al., 2017) and variants reported in ClinVar (Landrum et al., 2018) (**Tables 1**, **S2** and **S3)**.

Genome-wide CRISPR screens identify 46 common synthetic lethal genes

To study the connection between drug resistance and genes, we performed whole-genome loss-of-function screens in each of the five GemCis-resistant cell line derivatives. After transduction of the Brunello CRISPR-Cas9 knockout library (Doench et al., 2016a), we passaged the cells for 10 days to clear essential genes, then split into saline (PBS) or gemcitabine plus cisplatin treatment groups (**Figure 1A**). Each screen was performed at a drug concentration that allowed the GemCis-resistant cells to grow unrestricted, but which significantly inhibited the growth of the associated parental lines (**Table S1**). Screening parameters for each cell line are reported in **Table S4**. We measured sgRNAs 19 and 25 after transduction, which were 9 and 15 days after the start of treatment.

We defined genes as “synthetic lethal” with gemcitabine plus cisplatin treatment as those for which the combined cognate sgRNA counts were significantly lower (moderated t-test, FDR < 0.05) in the gemcitabine plus cisplatin-treated arm compared to the PBS arm when including both days 19 and 25 in the statistical model (**Table S5**). We identified 235 synthetic lethal genes that were significant in KU1919-GemCis, 888 for T24-GemCis, 2099 for TCCSUP-GemCis, 2369 for 253J-GemCis, and 511 for 5637-GemCis. Next, we performed gene set enrichment analysis (Korotkevich et al., 2019) on the full ranked list of genes according to their synthetic lethality. For this analysis, we combined the results to create one ranked gene list by including each of the five cell types in the statistical model directly. As expected, we found that the top ranked pathways were dominated by processes such as DNA repair, Fanconi Anemia, nucleotide excision repair, double-stranded break repair, base-excision repair, and DNA damage bypass mechanisms (**Figure 1B** and **Table S6**). These results are consistent with the known roles of DNA damage detection and repair in cisplatin resistance (Drayton and Catto, 2012; Galluzzi et al., 2012).

Next, we sought to identify the most robust and commonly synthetic lethal candidate genes by identifying only those significant in all 5 cell lines (**Figures 1C** and **S2**). Of the 46 commonly synthetic lethal genes, and illustrated in **Figure 1D**, some increased cell growth in PBS treatment, then reduced growth in gemcitabine plus cisplatin treatment. Other genes had very little impact on cell growth in PBS treatment, but then reduced growth when treated with gemcitabine plus cisplatin. Finally, some genes reduced cell growth in PBS treatment and further reduced growth with gemcitabine plus cisplatin treatment. As expected, nearly all 46 common synthetic lethal candidate genes fell into DNA damage response and repair pathways.

NPEPPS is a novel determinant of response to cisplatin

A recent systematic analysis of hundreds of CRISPR screens in cancer cell lines with comprehensive multi-omic profiling demonstrated that transcript expression markers were the best predictors of gene dependency (Dempster et al., 2020), providing rationale for the use of pre-treatment -omic profiling as a means to study the biological impact of synthetic lethal hits. Hence, to prioritize the 46 common synthetic lethal genes for validation and detailed mechanistic understanding, we performed RNA sequencing and mass spectrometry-based proteomic profiling on cell lysates of all cell lines grown in drug-free media (**Figure 1A**).

We investigated the transcriptome and proteome data by comparing parental to matched drug resistant derivative lines (-Gem, -Cis, and -GemCis) and identified several known mechanisms of chemoresistance. For example, acquired resistance to gemcitabine follows a number of common pathways across multiple tumor types that disrupt intracellular metabolism, such as the loss of deoxycytidine kinase (DCK) or increased expression of ribonucleotide reductase subunit M1 (RRM1) (Bepler et al., 2006; Bergman et al., 2005; Jordheim et al., 2011) (**Figure S3A**). Our data shows that RRM1 is specifically and significantly upregulated in nearly all Gem- and GemCis-resistant derivatives in the T24, TCCSUP, KU1919, and 5637 cell line series by both RNA and protein expression. In addition, and with the TCCSUP-GemCis line being the only exception, we found RRM1 copy number amplified, but not in the parental or the cisplatin resistant cells, providing strong support that a robust and consistently acquired mechanism of gemcitabine resistance in these cells is the copy number amplification and subsequent upregulation of RRM1 (**Figure S3B**). RRM1 is defined as an essential gene in the Dependency Map (Tsherniak et al., 2017), which we also detected in our screen (**Table S7**). Interestingly, in 253J-Gem and 253J-GemCis cell lines, which had minor changes in RRM1 expression, DCK expression was lost at the RNA and protein level with these results being supported by a copy number loss specific to these cells (**Figure S3B**).

Next, we analyzed gene and protein expression together while treating the cell line as a covariate in the statistical model. We found 1557 significantly upregulated genes across the Gem-resistant lines, 1897 in the Cis-resistant lines, and 1530 in the GemCis-resistant lines (moderated t-test, FDR < 0.05; **Table S8**). The proteomics data revealed 9 significantly upregulated proteins across the Gem-resistant cell lines, 1 in the Cis-resistant cell lines, and 10 in the GemCis-resistant cell lines (moderated t-test, FDR < 0.25; **Table S9**). Given the lower number of significant proteins and the relevance of transcript expression in predicting genetic dependency (Dempster et al., 2020), we first investigated the overlap between the CRISPR screen results and the transcriptomes from each of the resistant cell line derivatives compared to the parental cells. Few genes were significantly and consistently upregulated across the resistant derivatives in the list of 46 commonly synthetic lethal genes (**Figure 2A**). The most significantly and consistently upregulated genes were involved in DNA damage response and repair mechanisms, including ERCC6, XPA, REV1, POLH, ERRC8, PRIMPOL, NBN, and members of the Fanconi Anemia pathway. Puromycin sensitive aminopeptidase, NPEPPS, was identified as being the most consistently upregulated gene across the resistant derivatives (**Figure 2A, B**). We similarly found protein levels to be consistently and significantly upregulated (**Figure 2C**). NPEPPS was also a top synthetic lethal hit (**Figure 2D** and **Table S5**). Consistent with the proteomics results, immunoblotting for NPEPPS revealed that it was upregulated in the Cis-resistant and GemCis-resistant lines, with the Gem-resistant lines showing variable upregulation (**Figure 2E**).

We examined an independent whole-genome CRISPR screen that tested 27 general genotoxic agents (Olivieri et al., 2020) and here report new findings in support of NPEPPS as a novel mediator of cisplatin resistance. We found that cells with NPEPPS loss were specifically depleted in response to cisplatin, but not gemcitabine (**Figure 3A**). This result strongly supports the robustness of our findings as Olivieri et al. used different CRISPR libraries (TKOv2 and TKOv3) and cell line (retinal pigment epithelium-1, RPE1). Moreover, our screen results for all five cell lines were highly correlated with the three cisplatin screens (**Figure S4A**). Strikingly, nearly all 46 hits were significant hits associated with cisplatin, but not gemcitabine in Olivieri et al. (**Figure S4B**).

To validate our screen findings that NPEPPS depletion enhances sensitivity to gemcitabine plus cisplatin treatment in GemCis-resistant BCa cells, and parse its role in both cisplatin and gemcitabine resistance, we generated stable NPEPPS shRNA knockdowns in the KU1919-GemCis cell line (**Figure 3B**). The KU1919-GemCis line was selected for further experiments throughout this work because it had the strongest combination of a synthetic lethal result and gene/protein upregulation (**Figure 2**). We found that NPEPPS knockdown preferentially increased cisplatin, but not gemcitabine sensitivity (**Figure 3C, D**). The same result was found using siRNA in the KU1919-GemCis cell line and shRNA and/or siRNA in T24-GemCis and 253J-GemCis cells (**Figure S5**). We also found NPEPPS mRNA increased with cisplatin treatment in both KU1919-parental and KU1919-GemCis cells after 24 hours of treatment (**Figure 3E**). These results indicate that NPEPPS mediates sensitivity to gemcitabine plus cisplatin primarily by its effect on resistance to cisplatin.

Several agents inhibit NPEPPS activity (Drinkwater et al., 2017). Tosedostat, an orally available M1 aminopeptidase prodrug has antileukemic activity with a favorable toxicity profile in patients (CHR-2797, CAS 238750-77-1) (Cortes et al., 2013; van Herpen et al., 2010; Krige et al., 2008; Löwenberg et al., 2010; Mawad et al., 2016). We tested the response of the KU1919-GemCis, T24-GemCis, and TCCSUP-GemCis resistant cells to serial doses of tosedostat at the resistant doses of gemcitabine, cisplatin, and gemcitabine plus cisplatin. Consistent with NPEPPS depletion, tosedostat did not sensitize cells to gemcitabine (**Figure 3F** and **Table S1)**. The strongest combined effect was seen with cisplatin and gemcitabine plus tosedostat treatment (**Figure S6)**. These results show that GemCis-resistant BCa cells can be re-sensitized to cisplatin-based treatments at varying degrees by genetic and pharmacologic inhibition of NPEPPS.

Volume regulated anion channels and their impact on chemoresistance in bladder cancer cells

NPEPPS is one of 13 M1 aminopeptidases that cleaves amino acids from the N-terminus of polypeptides. NPEPPS is involved in cell growth, development and antigen presentation (Constam et al., 1995; Menzies et al., 2010; Saric et al., 2004; Towne et al., 2008). A role of NEPPPS in chemotherapeutic response is yet to be described. To begin characterizing the mechanisms NPEPPS uses to drive cisplatin resistance, we investigated NPEPPS protein interaction partners in the BioPlex interactome, a database that has collected affinity-purification mass spectrometry measurements of systematically over-expressed, tagged proteins (Huttlin et al., 2020). Remarkably, among the small number of proteins that were observed to interact with NPEPPS, were all five members of the volume regulated anion channel (VRAC), leucine rich repeat containing 8 VRAC subunit A-E (LRRC8A-E) (**Figure 4A**). Supporting this finding, other affinity-purification mass spectrometry experiments independently reported the interaction between NPEPPS and VRAC members across different cell lines (Kasuya et al., 2018; Syeda et

al., 2016). Equally interesting was that none of the other 12 M1 aminopeptidases were found in complex with any VRAC members in the BioPlex interactome.

VRACs directly respond to osmotic stress by trafficking osmolytes such as chlorine, potassium, and taurine, across the plasma membrane to regulate cell volume (Voss et al., 2014). Importantly, subunits LRRC8A and LRRC8D are mediators of platinum drug resistance in chronic myelogenous leukemia cells. Knockout experiments in kidney and colorectal cell lines showed that 50-70% of intracellular cisplatin is transported through these channels (Planells-Cases et al., 2015a), mediated by LRRC8A and LRRC8D. Similar findings were subsequently found in ovarian cancer and alveolar carcinoma cell lines (Sørensen et al., 2014, 2016a, 2016b). Thus, we focus on the LRRC8A and LRRC8D subunits for further analysis.

We revisited our CRISPR screens and RNAseq data to determine if loss of LRRC8A and/or LRRC8D impacted cisplatin resistance. As predicted, LRRC8A and LRRC8D loss provided a growth advantage to cells treated with gemcitabine plus cisplatin (**Figure 4B, C**). Most strikingly, LRRC8A was the 1st and LRRC8D was the 11th ranked gene that when lost provided a growth advantage in gemcitabine plus cisplatin treatment (**Figure 4D**). LRRC8A and/or LRRC8D mRNA expression was reduced for most of the Cis- or GemCis-resistant cell lines, with the Gem-resistant lines showing variable differential expression (**Figure 4E, F**). Most notable, LRRC8D gene expression in the TCCSUP-Cis and TCCSUP-GemCis cells was completely lost (**Figure 4F**). We found that in these cell lines, there is a deep deletion at the LRRC8D locus (**Figure S7**). NPEPPS loss in the TCCSUP-GemCis lines showed the weakest synthetic lethal result compared to the other four GemCis-resistant lines (**Figure 2D**) and LRRC8D loss had no effect on TCCSUP-GemCis growth (**Figure 4C**), while LRRC8A loss did in fact increase growth (**Figure 4B**). Taken together, these data support a functional dependency between NPEPPS and VRAC subunits LRRC8A and LRRC8D in relation to cisplatin resistance.

Given that VRACs transport cisplatin and carboplatin (Planells-Cases et al., 2015a) and finding NPEPPS in complex with LRRC8A and LRRC8D (Huttlin et al., 2020; Kasuya et al., 2018; Syeda et al., 2016), we hypothesized that NPEPPS may be a negative regulator of VRAC activity, consequently reducing import of intracellular cisplatin. Thus, we tested the impact of NPEPPS on osmolytes known to be transported through VRACs. NPEPPS knockdown in KU1919-GemCis-shN39 cells resulted in a significantly lower levels of intracellular taurine, hypotaurine, creatine, phosphocreatine, and several other amino acids (**Figure 4G** and **Table S10**), which are known to be exported via VRACs. In addition, intracellular levels of taurine were reduced even further when cells with knockdown of NPEPPS were also treated with 10μM cisplatin, which is the resistance dose for the KU1919-GemCis cells (**Figure 4H**). This suggests that cisplatin further stimulates channel activity when NPEPPS is decreased, which allows for increased export of taurine, and as we show next increases cisplatin import.

To evaluate NPEPPS impact on cisplatin import, we directly measured intracellular cisplatin using the metal ion detection capabilities of mass cytometry (Chang et al., 2015). Intracellular cisplatin was measured after 4 hours of treatment at 10μM for KU1919-parental, KU1919-GemCis, and KU1919-GemCis-shN39 cells. As expected, KU1919-GemCis cells showed decreased uptake of cisplatin compared to KU1919-parental cells. Knockdown of NPEPPS shifted the intracellular levels of cisplatin to be nearly double (median Pt 195 = 77) of the GemCis-resistant cells (median Pt 195 = 44.5) and half of the parental cells (median Pt 195 = 158), suggesting that NPEPPS depletion allows increased import of cisplatin (**Figure 4I** and **S8A,B**).

Furthermore, we measured protein levels of LRRC8A and LRRC8D after 48 hours of PBS or 10μM cisplatin treatment in NPEPPS knockdown or nontargeting control KU1919-GemCis cells. Supporting the mass cytometry results (**Figure 4I**) and the result that taurine is exported at a higher rate upon cisplatin stimulation in the KU1919-GemCis-shN39 cells (**Figure 4H**), NPEPPS knockdown increased DNA damage as measured by increased γH2AX foci (**Figure 4J** and **S8C**). However, we did not find major changes in LRRC8A or LRRC8D expression in response to NPEPPS knockdown or cisplatin treatment (**Figure 4J** and **S8C**). Taken together, these data and previous studies, support a role for NPEPPS in regulating cellular osmolyte homeostasis via an interaction with VRACs.

Genetic and pharmacologic inhibition of NPEPPS enhances chemotherapy sensitivity *in vivo* and in patient tumor-derived organoids

To test if NPEPPS depletion would sensitize tumor cells to gemcitabine plus cisplatin treatment *in vivo*, we established subcutaneous xenografts using the KU1919-GemCis cells with either NPEPPS shRNA knockdown or non-targeting shRNA control. When tumors reached roughly 200mm^3, mice were randomized into four groups: shCtrl1 with PBS, shCtrl1 with gemcitabine plus cisplatin, shN39 with PBS, and shN39 with gemcitabine plus cisplatin. Treatment was delivered through intraperitoneal injection, with PBS or gemcitabine plus cisplatin administered three times weekly for four weeks. Tumor volumes were monitored until they reached the predetermined endpoint of 2cm^3. NPEPPS knockdown alone and gemcitabine plus cisplatin treatment alone had significant impact on tumor growth compared to vehicle-treated, shRNA controls. The combination of NPEPPS knockdown and gemcitabine plus cisplatin treatment led to an even stronger and more significant impact on tumor growth (**Figure 5A**). We further analyzed tumor growth using linear mixed-effects models aimed at capturing trends in tumor volume change in relation to pre-treatment baseline tumor volume across the four groups. According to this model, tumor growth inhibition by NPEPPS knockdown (p=0.00178), GemCis treatment (p=5.49e-7), or the combination of NPEPPS knockdown and gemcitabine plus cisplatin treatment (p=1.47e-8) were all consistent effects over the treatment period (**Figure S9A, B**). We validated NPEPPS knockdown in the pre-xenograft inoculate cells and after tumors were removed from mice upon reaching the 2cm^3 endpoint (**Figure S9C**). Survival analysis using tumor volume as the endpoint showed that mice treated with gemcitabine plus cisplatin had a 14-day survival advantage. Similarly, knockdown of NPEPPS resulted in a 14-day survival advantage. Mice treated with gemcitabine plus cisplatin and with NPEPPS knockdown tumors had a 25-day survival advantage, a statistically significant improvement (Logrank test, p<0.0001) (**Figure 5B**).

Next, we extended our work to evaluate the impact of the drug combination of tosedostat and cisplatin on *ex vivo* patient tumor-derived BCa organoids. We generated three independent organoid models from patient cystectomy samples that did not respond to gemcitabine plus cisplatin NAC (**Figure S10A**). Based on targeted mutations or global copy number alterations, the organoids had similar characteristics of the tumor tissues from which they were derived (**Figure S10B, C**). We treated the organoids with cisplatin and tosedostat for six days and then removed the drugs to allow recovery for 10 days (**Figure S10D)**. Cisplatin with tosedostat resulted in significant decreases in viability across all organoids (**Figures S11-S13**). Viability of vehicle control and tosedostat treated organoids show an initial decrease of roughly 20%, but these cells recover over time to be equal to the vehicle control. We saw no different in 5μM or 20μM tosedostat (**Figure S11D**). After 10 days of recovery from treatment, organoids were reseeded at different densities based on overall growth and allowed to re-establish and grow for an additional 6 days, then cell viability was assessed (**Figures 5C-E** and **S11-13**). Treatment

with increasing concentrations of Cis alone resulted in a progressively decreased viability of organoids. Strikingly, the addition of tosedostat to cisplatin resulted in further reductions at concentrations in which cisplatin treatment alone had minor effects (**Figure 5C-E**). Notably, the combined treatment with tosedostat lowered the effective concentration to 2μM in patients 1 and 2, and to 25μM in the highly treatment resistant patient 3 (**Figure 5C-E**). These findings are translationally relevant since the maximum concentration of cisplatin in patients is 14μM (Liston and Davis, 2017) and provide additional validation using a human-derived model system that tosedostat enhances cisplatin activity.

The increase in NPEPPS mRNA that has been observed in response to chronic (**Figure 2B, C**) and acute cisplatin treatment *in vitro* and in the *ex vivo* organoids (**Figure 3E**) suggests that high levels of NPEPPS expression are part of an acquired or adaptive rather than intrinsic mechanism of drug resistance in tumors that have been exposed to cisplatin. Hence, pre-treatment tumor NPEPPS levels may not necessarily be a biomarker of chemotherapy response in bladder cancer. However, given the relationship of NPEPPS to VRACs described previously and findings that levels of LRRC8A and LRRC8D are predictive of cisplatin response in ovarian cancer (Planells-Cases et al., 2015a), we reasoned that such relationships would also be true in BCa. Using TCGA data from muscle invasive bladder cancer (Robertson et al., 2017), we compared patients with and without a record of platinum-based treatment (Goodspeed et al., 2019) with respect to amplification, copy number, and expression of either LRRC8A or LRRC8D. Notably, patients with LRRC8A and/or LRRC8D copy number gain or overexpression that received platinum-based treatment showed significantly improved overall survival in contrast to those with no record of this treatment modality (**Figure 5F**, **G**). Together, these findings support VRAC subunits LRRC8A and LRRC8D as pre-treatment biomarkers of response to cisplatin-based chemotherapy (Rottenberg et al., 2021).

DISCUSSION

NPEPPS has been suggested to play a role in a range of cellular processes including promoting autophagy, regulating cell cycle progression, and antigen processing (Constam et al., 1995; Menzies et al., 2010; Saric et al., 2004; Towne et al., 2008). The majority of what is known about NPEPPS has been from studies in the brain, where it targets the degradation of polyglutamine sequences and misfolded protein aggregates associated with a number of neurodegenerative diseases, including Alzheimer's disease, Huntington's Disease, and Parkinson's disease (Karsten et al., 2006; Kudo et al., 2011; Menzies et al., 2010; Schönlein et al., 1994; Yanagi et al., 2009). As reported in gnomAD, NPEPPS is a highly conserved gene and constrained based on several metrics of intolerance to genetic variation in the population (Karczewski et al., 2020). NPEPPS is also ubiquitously expressed across human tissues (Uhlen et al., 2017). However, despite these features, genetic modification in mice is tolerable (Osada et al., 1999; Towne et al., 2008) and as we have shown from our CRISPR screen results, knockout is not essential (**Figure 2D**). Overall, NPEPPS presents a viable therapeutic target and we have shown that its downregulation genetically or pharmacologically re-sensitizes treatment-resistant cells back to cisplatin.

Broadly, aminopeptidases have been therapeutically targeted as potential cancer treatments (Hitzerd et al., 2014). More specifically, NPEPPS is a zinc containing M1 aminopeptidase. Tosedostat was developed as a target of M1 aminopeptidases and the intracellular metabolized product CHR-79888 is the most potent inhibitor of NPEPPS reported (Krige et al., 2008; Reid et al., 2009). There have been a total of 11 clinical trials with tosedostat as reported in *clinicaltrials.gov* (Cortes et al., 2013; van Herpen et al., 2010; Krige et al., 2008; Löwenberg et al., 2010; Mawad et al., 2016). The focus of its application has been in leukemias and myelomas, with several applications in solid tumors. The few clinical trials completed have reported tosedostat as being well tolerated by patients, but with modest effect as a cancer treatment alone. A few examples of tosedostat in combination with cytarabine, azacitidine, capecitabine or paclitaxel have been tried, but there are no reports of tosedostat being tried in combination with platinum-based chemotherapy, supporting the novel application of cisplatin-based chemotherapy plus tosedostat that we propose in this study.

Another exciting potential application of NPEPPS inhibition is to provide alternative treatment options for BCa patients. Many patients are ineligible for cisplatin-based chemotherapies, leaving them with less effective options, such as carboplatin. VRACs also transport carboplatin at similar amounts as cisplatin (Planells-Cases et al., 2015a), thus combining an NPEPPS inhibitor, such as tosedostat, with carboplatin could provide a more effective and less toxic drug combination option for cisplatin ineligible patients. A further area of novel development would be the impact of NPEPPS inhibition on ICT with its known effect on MHC class I antigen presentation on dendritic cells (Towne et al., 2008). ERAP1 and ERAP2, other M1 aminopeptidases in the same family as NPEPPS, have been linked to boosting T cell and NK cell mediated immune response in cancer (Compagnone et al., 2019); however the impact of NPEPPS on antigen presentation in tumor cells is yet to be investigated. Interestingly, low ERAP2 was associated with improved response to anti-PD-L1 in luminal bladder cancer (Lim et al., 2018). The impact of NPEPPS inhibition in immunotherapies requires further study.

The data we provide supports the role of NPEPPS and VRACs in cisplatin-based response in BCa, thus we have scoped our conclusions to BCa. However, results outside of this study support a molecular mechanism with broader impact. The evidence that supports the interaction between NPEPPS and VRACs were derived from several different cell types and the evidence that implicates VRACs in platinum-based chemotherapy sensitivity is from ovarian cancer

(Planells-Cases et al., 2015b; Sørensen et al., 2014, 2016a, 2016b). If the NPEPPS-VRAC mechanism of platinum-based chemotherapy resistance is a general mechanism, then there are clear implications for any cancer type that uses platinum-based treatments. Hence, we can propose a hypothetical model (**Figure 6**) where a cancer cell imports cisplatin, which in turn causes DNA damage and eventually cell death. An inherent mechanism of resistance can simply be the number of VRACs in a tumor cell, where downregulation of VRAC subunits can lead to treatment resistance, such as was previously found in ovarian cancer, or the opposite effect seen with LRRC8A or LRRC8D upregulation in BCa (**Figure 5F, G**). In our model, NPEPPS interacts with LRRC8A and/or LRRC8D to inhibit channel activity, thus providing resistance to cisplatin and overall chemoresistance. If proven to be true, our insight into this mechanism opens up opportunities for novel therapeutic strategies to reverse or prevent the development of cisplatin resistance, such as the development of agents that block NPEPPS interactions with VRACs.

This work is not without its limitations. There is strong evidence from independent studies with multiple different cell lines and experimental techniques that NPEPPS and VRAC subunit proteins interact (Huttlin et al., 2020; Kasuya et al., 2018; Syeda et al., 2016). It would be very surprising this would not be the case for BCa. We have also shown in multiple settings that inhibiting NPEPPS genetically or pharmacologically results in re-sensitizing resistant BCa cells to cisplatin. However, where and when NPEPPS interacts with VRACs in the cell is yet to be determined. In addition, NPEPPS could have effects on treatment response outside of the VRACs. Our work is also limited by the fact that we have not shown that NPEPPS depletion leads directly to carboplatin sensitization in BCa, but that is likely given the known VRAC relationships (Planells-Cases et al., 2015a). Despite these study limitations, the implications of NPEPPS as a therapeutic target for better treatment response has the potential to be translated into novel treatment regimens for improved patient outcomes.

In conclusion, our finding that NPEPPS mediates cisplatin-based chemoresistance is both novel and actionable. We provided *in vitro*, *in vivo*, and *ex vivo* evidence that this mechanism is robust and therapeutically targetable. Future directions will include determining the detailed mechanism of NPEPPS-mediated treatment response, particularly though the interaction with VRACs, and generating additional pre-clinical data testing NPEPPS inhibitor efficacy and toxicities. Cisplatin-based chemotherapeutic regimens are mainstays of treatment across many cancer types and these novel findings lay the groundwork for improved treatment of patients harboring these tumors (Rottenberg et al., 2021). Our findings also have implications into other platinum agents, such as carboplatin which would further improve efficacy of this agent in additional cancer types. Finally, for the benefit of the research community, we make the -omic and CRISPR screen data publicly available through an R Shiny app (https://bioinformatics.cuanschutz.edu/GC_Visualization/) which will provide a rich source for novel analysis in the mechanisms of chemotherapy resistance.

Materials and Methods

Key Resource Table

REAGENT or RESOURCE	SOURCE	IDENTIFIER
Antibodies		
NPEPPS	Invitrogen	PA5-22383
NPEPPS	Invitrogen	PA5-83788
GAPDH (D16H11) XP Rabbit mAb	Cell Signaling Technologies	5174S
Anti-LRRC8A, Rabbit polyclonal	LSBio	LS-B16989
Anti-LRRC8D, Rabbit polyclonal	SinoBiological	104245-T32
Phospho-Histone H2A.X (Ser139) Monoclonal Antibody (3F2)	Invitrogen	MA1-2022
Anti-mouse IgG (whole molecule), peroxidase antibody in rabbit	Sigma-Aldrich	A9044
Anti-rabbit IgG (whole molecule), peroxidase-conjugated (HRP)	MP Biomedicals	855689
Bacterial and Virus Strains		
Library Efficiency™ DH5α competent cells	ThermoFisher	18263012
Endura™ ElectroCompetent cells	Lucigen	60242
Chemicals, Peptides, and Recombinant Proteins		
Gemcitabine hydrochloride	Sigma	Y0000675
Gemcitabine hydrochloride (mouse experiment)	BOC Sciences	122111-03-9
Cisplatin	Sigma	PHR-1624
Cisplatin (mouse experiment)	Sigma	11344357
Tosedostat	Sigma	SML2303
Tosedostat (mouse experiment)	BOC Sciences	BCMV18265-2B
Tosedostat (organoids)	Tocris	3595
Puromycin dihydrochloride	Sigma	P9620
Fetal Bovine Serum (FBS)	VWR Seradigm Life Sciences	89510-186
RIPA Lysis and Extraction Buffer	ThermoFisher	89900
T-PER™ Tissue Protein Extraction Reagent	ThermoFisher	PI78510
Halt™ Protease and Phosphatase Inhibitor Cocktail, EDTA-free (100X)	ThermoFisher	PI78443
Polybrene [10mg/mL]	EMD Millipore	TR-1003-G
Lipofectamine 3000 Reagent	ThermoFisher	L3000075
Polyethylenimine, linear (PEI)	Polysciences, Inc.	23966
Lipofectamine® RNAiMAX Reagent	ThermoFisher	13778075
0.5% Trypsin-EDTA (10x)	Gibco	15400-54
DPBS (1x)	Gibco	14190-144
4% formalin	Sigma	HT501128
2.5% Low-Melting Agarose	Sigma	2070
Herculase II Fusion Enzyme	Agilent	600679
DNAseI	Invitrogen	18068015
Deoxynucleotide (dNTP) Solution Mix	New England Biolabs	N0447L
Critical Commercial Assays		
Puregene Cell and tissue Kit	Qiagen	158388
RNase A Solution	Qiagen	158924

SureSelect Human All Exon v6	Agilent	G9611
Amersham ECL Rainbow Marker -Full Range	Sigma	RPN8000E
Precision Plus Protein™ Kaleidoscope™ Prestained Protein Standards	Biorad	1610375
SuperSignal West Pico Plus	ThermoFisher	34580
SuperSignal West Fempto	ThermoFisher	34094
4–20% Mini-PROTEAN® TGX™ Precast Protein Gels	Biorad	4561096, 4561094
4X Protein Sample Loading Buffer for Western Blots	LI-COR	928-40004
KAPA library Quant Kit ROX Low	Kapa Biosystems	KK4873
Pierce™ BC Protein Assay Kit	ThermoFisher	23225
Universal Plus mRNA –Seq +UDI kit	Nugen Technologies	9144-96
RNAEasy Plus	Qiagen	74106
QIAmp DNA Mini-Kit	Qiagen	51304
Cell-ID 20-plex Pd Barcoding Kit	Fluidigm	201060
MycoAlert	Lonza	LT07-318
SensiFAST Probe No-ROX Mix	Bioline	BIO-86005
SuperScript™ II Reverse Transcriptase	Invitrogen	18064022
NPEPPS TaqMan® Gene Expression Assay	Thermofisher	Hs00196905_m1
HMBS TaqMan® Gene Expression Assay	Thermofisher	Hs00609297_m1
alamarBlue™ Cell Viability Reagent	Invitrogen	DAL 1025
Biorad Protein Assay Dye reagent concentrate	Biorad	5000006
Deposited Data		
Raw RNA sequencing data	This paper	GEO:XX
Raw whole exome sequencing	This paper	GEO:XX
Affymetrix GSA V3 organoid CAN	This paper	GEO:XX
Raw mass spectrometry proteomics	This paper	Peptide Atlas:XX
CRISPR screening results	This paper	**Table S13**
Bladder tumor proteomics	ProteomeXchange	PXD010260
TCGA bladder cancer patient gene expression	cBioPortal	https://cbioportal-datahub.s3.amazonaws.com/blca_tcga_pub_2017.tar.gz
TCGA bladder cancer survival data	(Goodspeed et al., 2019)	Supplementary Table 4
DepMap Common essential and non-essential genes (20Q1)	https://depmap.org/portal/download	common_essentials.csv, nonessentials.csv
Experimental Models: Cell Lines		
T24 parental	Resistant Cancer Cell Line Collection (https://research.kent.ac.uk/industrial-biotechnology-centre/the-resistant-cancer-cell-line-rccl-collection/)	N/A
T24 gemcitabine resistant		N/A
T24 cisplatin resistant		N/A
T24 gemcitabine and cisplatin resistant		N/A
TCCSUP parental		N/A
TCCSUP gemcitabine resistant		N/A
TCCSUP cisplatin resistant		N/A
TCCSUP gemcitabine and cisplatin resistant		N/A
253J parental		N/A
253J gemcitabine resistant		N/A

253J cisplatin resistant		N/A
253J gemcitabine and cisplatin resistant		N/A
KU1919 parental		N/A
KU1919 gemcitabine resistant		N/A
KU1919 cisplatin resistant		N/A
KU1919 gemcitabine and cisplatin resistant		N/A
5637 parental		N/A
5637 gemcitabine resistant		N/A
5637 cisplatin resistant		N/A
5637 gemcitabine and cisplatin resistant		N/A
293FT	ThermoFisher	R70007
Experimental Models: Organisms/Strains		
Mouse: Nu/J (JAX)	The Jackson Laboratory	002019
Oligonucleotides		
CRISPR screening library primers	**Table S11**	N/A
Recombinant DNA		
Human CRISPR Knockout Pooled Library (Brunello) - 1 vector system (lentiCRISPRv2)	Addgene	73179
psPAX2	Addgene	12260
pMD2.G	Addgene	12259
shCtrl1	University of Colorado Functional Genomics Facility	SHC002
shCtrl2	University of Colorado Functional Genomics Facility	SHC016
shN38	University of Colorado Functional Genomics Facility	TRCN0000073838
shN39	University of Colorado Functional Genomics Facility	TRCN0000073839
shN40	University of Colorado Functional Genomics Facility	TRCN0000073840
Software and Algorithms		
BWA-MEM (0.7.17)	(Li, 2013)	http://bio-bwa.sourceforge.net
Samblaster (0.1.24)	(Faust and Hall, 2014)	https://github.com/GregoryFaust/samblaster
Samtools (1.8)/HTSlib (1.9)	(Li et al., 2009)	http://www.htslib.org/
GATK Base Quality Score Recalibration (BQSR)	GATK4 v4.1.8	https://gatk.broadinstitute.org/hc/en-us/articles/360035890531-Base-Quality-Score-Recalibration-BQSR-
Calling Somatic SNVs and Indels with Mutect2	(Benjamin et al., 2019)	https://www.biorxiv.org/content/10.1101/861054v1.full.pdf

Somatic copy number variants	GATK4 v4.1.8	http://genomics.broadinstitute.org/data-sheets/PPT_Somatic_CNV_WKST_ASHG_2016.pdf
The Nextflow (20.04.1) pipeline implementing the workflows for this paper	This paper	https://github.com/javaidm/layer_lab_vc
SavvyCNV: genome-wide CNV calling from off-target reads v0.10	(Laver et al., 2019)	https://www.biorxiv.org/content/10.1101/617605v1
BBTools	BBMap – Bushnell B. – sourceforge.net/projects/bbmap/	https://jgi.doe.gov/data-and-tools/bbtools/
Image Studio	LiCor	https://www.licor.com/bio/image-studio/
STAR (2.6.0a)	(Dobin et al., 2013)	https://github.com/alexdobin/STAR
FLowJo (10.7.1)	(FlowJo, 2019)	https://www.flowjo.com/
Biodiscovery Nexus CN7.5	N/A	https://www.biodiscovery.com/products/Nexus-Copy-Number
GenomeStudio (1.9.4)	Genotyping Module	https://www.illumina.com/techniques/microarrays/array-data-analysis-experimental-design/genomestudio.html
Limma R package (3.44.3)	(Ritchie et al., 2015)	https://bioconductor.org/packages/release/bioc/html/limma.html
edgeR R package (3.30.3)	(Robinson et al., 2010)	https://bioconductor.org/packages/release/bioc/html/edgeR.html
fgsea R package (1.14.0)	(Sergushichev, 2016)	https://bioconductor.org/packages/release/bioc/html/fgsea.html
ggplot2 R package (3.2.2)	(Wickham, 2009)	https://ggplot2.tidyverse.org/
ggpubr R package (0.4.0)	N/A	https://cran.r-project.org/web/packages/ggpubr/index.html
ClusterProfiler	(Yu et al., 2012)	https://bioconductor.org/packages/release/bioc/html/clusterProfiler.html

caRpools R package	(Winter et al., 2016)	https://cran.r-project.org/web/packages/caRpools/index.html
DEseq2 R package	(Love et al., 2014)	https://bioconductor.org/packages/release/bioc/html/DESeq2.html
Maven	(Clasquin et al., 2012)	http://genomics-pubs.princeton.edu/mzroll/index.php
openSWATH	(Röst et al., 2014)	http://openswath.org/en/latest/
vsn (3.12)	(Huber et al., 2002)	https://bioconductor.org/packages/release/bioc/html/vsn.html
lme4 (1.1-26)	(Bates et al., 2015)	https://cran.r-project.org/web/packages/lme4/index.html
lmerTest (3.1-3)	(Kuznetsova et al., 2017)	https://cran.r-project.org/web/packages/lmerTest/index.html
PyProphet	(Teleman et al., 2015)	http://openswath.org/en/latest/docs/pyprophet.html
MSstats R package	(Choi et al., 2014)	https://www.bioconductor.org/packages/release/bioc/html/MSstats.html
TRIC	(Röst et al., 2016)	https://github.com/msproteomicstools/msproteomicstools

Cell Culture

All human BCa cell lines as reported in the Key Resource Table were obtained from the Resistant Cancer Cell Line (RCCL) Collection and were grown in Iscove's Modified Dulbecco's Medium (IMDM) with 10% Fetal Bovine Serum (FBS). Cells were passaged every two to three days. Resistance to gemcitabine and cisplatin were confirmed at the reported resistance doses from the RCCL (**Table S1** and **Figure S1**). Lentivirus production utilized 293FT cells (ThermoFisher), which were maintained in DMEM (high glucose) supplemented with 0.1mM non-essential amino acids (NEAA), 6mM L-glutamine, 1mM sodium pyruvate, and 500μg/mL geneticin (G418) with 10% FBS added. Cells were routinely monitored for mycoplasma and confirmed negative at multiple times during this study using MycoAlert (Lonza). All cells were grown at 37°C with 5% CO_2 in a humidified incubator.

All molecular characterization efforts (RNA sequencing, whole exome sequencing, and mass spectrometric proteomics) were performed on cells from independent passages and in drug-free, complete media to identify stable molecular changes rather than treatment induced transient adaptations. Cells were routinely passaged through drug-containing media at the

resistant doses (**Table S1**) to confirm resistance was maintained and early passage cells were utilized whenever possible.

RNA sequencing

Sample preparation

All cell lines were grown for several passages in the absence of antibiotics, gemcitabine or cisplatin. Cell pellets were snap frozen from sub-confluent dishes from 3 separate passages (replicates) for each of the 20 cell lines sequenced (5 cell lines, each with 4 derivatives: parental, G-resistant, C-resistant, GC-resistant). RNA was extracted using the RNAeasy Plus Kit (Qiagen). Cells were lysed and passed through QIAShredder column (Qiagen) according to the manufacturer's protocol. gDNA elimination columns (Qiagen) were used to remove any residual gDNA from the purified RNA. RNA integrity was assessed on the High Sensitivity ScreenTape Assay on the Tape Station2200 (Agilent Technologies) and only samples with an RIN score of 8 or higher were used for sequencing. RNA library preparation was performed using the Universal Plus mRNA –Seq +UDI kit (Nugen Technologies) according to the manufacturer's specification. Each library was sequenced to a minimum of 40 million clusters or 80 million 150bp paired-end reads on a NovaSeq 6000 instrument (Illumina) at the University of Colorado Cancer Center Genomics Shared Resource.

Data processing

Illumina adapters and the first 12 base pairs of each read were trimmed using BBDuk and reads <50bp post trimming were discarded. Reads were aligned and quantified using STAR (Dobin et al., 2013) against the Ensembl human transcriptome (GRCh38.p12 genome (release 96)). Ensembl genes were mapped to HGNC gene symbols using HGNC and Ensembl BioMart. Gene counts were generated using the sum of counts for transcripts of the same gene. Lowly expressing genes were removed if mean raw count <1 or mean CPM (counts per million) <1 for the entire dataset. Reads were normalized to CPM using the edgeR R package (Robinson et al., 2010). Differential expression was calculated using the voom function in the limma R package (Ritchie et al., 2015). In addition to two-group comparisons, single drug comparisons for all cell lines were generated with cell line as a covariate (**Table S7**).

Alignment and transcript quantification

STAR --runThreadN 12 --runMode genomeGenerate --sjdbGTFfile Homo_sapiens.GRCh38.96.gtf --genomeFastaFiles Homo_sapiens.GRCh38.dna_sm.primary_assembly.fa

STAR --readFilesIn Read1.fastq.gz Read2.fastq.gz --readFilesCommand zcat --runThreadN 6 --alignEndsProtrude 13 ConcordantPair --outFilterScoreMinOverLread 0.66 --outFilterMatchNminOverLread 0.66 --outSAMtype BAM SortedByCoordinate --quantMode GeneCounts

Pathway analysis

Gene set enrichment analysis was performed using the full list of genes ranked by fold change for the indicated comparison and the fgsea R package (Sergushichev, 2016) using gene sets from the Molecular Signatures Database (v7.0) (Liberzon et al., 2011). Over representation analysis was performed using the ClusterProfiler R package with genes less than an adjusted p-value 0.05 (Yu et al., 2012) or Metascape (Zhou et al., 2019). General plots were generated

with the ggplot2 and ggpubr R packages (Wickham, 2009). Heatmaps were generated with the ComplexHeatmap R package following z-score transformation (Gu et al., 2016).

Proteomics

Sample preparation

All cell lines were grown for several passages in the absence of antibiotics, gemcitabine or cisplatin, then seeded at 100,000 – 200,000 cells per well and grown for 48 hours in IMDM + 10% FBS. Approximately 48 hours after seeding cells the supernatant was aspirated and cells were washed 3 times with cold phosphate buffered saline (PBS). Cells were lysed in 100µl of 8M Urea, 50mM Tris-HCl, pH 8.0. Lysates were transferred to pre-chilled 1.5mL microcentrifuge tubes and centrifuged at 15000 RCF for 10 minutes to pellet. The supernatant was then transferred to a clean, pre-chilled tube and frozen. Lysate replicates were collected in triplicate from different passages. Cell pellets were lysed in 8M Urea supplemented with 0.1% Rapigest MS compatible detergent. DNA was sheared using probe sonication, and protein concentration was estimated by BCA (Pierce, Thermo Scientific). A total of 30µg protein per sample was aliquoted, and samples were diluted to <2M Urea concentration using 200mM ammonium bicarbonate while also undergoing reduction with DTT (10mM) and then alkylation with IAA (100mM). The pH of diluted protein lysates was verified as between 7-8, and samples were digested with sequencing grade Trypsin/Lys-C enzyme (Promega) in the presence of 10% Acetonitrile for 16 hours at 37°C. Samples were acidified adding formic acid to 1%, and speed vac dehydration was used to evaporate acetonitrile. Peptides were desalted on C18 tips (Nest group) and dried to completion. Prior to MS, peptides were resuspended in 0.1% Formic Acid solution at 0.5µg/µL concentration with 1:40 synthetic iRT reference peptides (Biognosys).

Data acquisition

Peptides were analyzed by liquid chromatography coupled with mass spectrometry in data independent acquisition (DIA) mode essentially as described previously (Robinson et al., 2020). Briefly, 4µL of digested sample were injected directly unto a 200 cm micro pillar array column (uPAC, Pharmafluidics) and separated over 120 minutes reversed phase gradient at 1200 nL/min and 60°C. The gradient of aqueous 0.1% formic acid (A) and 0.1% formic acid in acetonitrile (B) was implemented as follows: 2% B from 0 to 5 min, ramp to 4% B at 5.2 minutes, linear ramp to 28% B at 95 minutes, and ramp to 46% B at 120 minutes. After each analytical run, the column was flushed at 1200 nL/min and 60°C by injection of 50% Methanol at 95% B for 25 minutes followed by a 10 minutes ramp down to 2% B and a 5 minute equilibration to 2% B. The eluting peptides were electro sprayed through a 30 um bore stainless steel emitter (EvoSep) and analyzed on an Orbitrap Lumos using data independent acquisition (DIA) spanning the 400-1000 m/z range. Each DIA scan isolated a 4 m/z window with no overlap between windows, accumulated the ion current for a maximum of 54 seconds to a maximum AGC of 5E5, activated the selected ions by HCD set at 30% normalized collision energy, and analyzed the fragments in the 200-2000m/z range using 30,000 resolution (m/z = 200). After analysis of the full m/z range (150 DIA scans) a precursor scan was acquired over the 400-1000 m/z range at 60,000 resolution.

Peptide library generation

To construct a comprehensive peptide ion library for the analysis of human BCa we combined several datasets, both internally generated and external publicly available data resources were utilized. First, we utilized a previously published (Berle et al., 2018) human bladder tumor proteomics experiment by downloading raw files from the online data repository

(ProteomeXchange, PXD010260) and searching them through our internal pipeline for data dependent acquisition MS analysis (Parker et al., 2016) against the uniprot human reviewed canonical sequence database, downloaded July 2019, using internal peptides to perform retention time alignment (Parker et al., 2015). To this library, we appended a sample specific library generated from DIA-Umpire extraction of pseudo-spectra from one full set of replicates from the experimental bladder tumor cell lines. A final, combined consensus spectrast library containing all peptide identifications made between the internal and external dataset was compiled and decoy sequences were appended.

Data analysis

Peptide identification was performed as previously described in (Parker et al., 2015, 2016). Briefly, we extracted chromatograms and assigned peak groups using openSWATH (Röst et al., 2014) against the custom BCa peptide assay library described above. False discovery rate for peptide identification was assigned using PyProphet (Teleman et al., 2015) and the TRIC (Röst et al., 2016) algorithm was used to perform feature-alignment across multiple runs of different samples to maximize data completeness and reduce peak identification errors. Target peptides with a false discovery rate (FDR) of identification <1% in at least one dataset file, and up to 5% across all dataset files were included in the final results. We used SWATH2stats to convert our data into the correct format for use with downstream software MSstats27. Each individual data file was intensity normalized by dividing the raw fragment intensities to that files total MS2 signal. MSstats (Choi et al., 2014) was used to convert fragment-level data into protein-level intensity estimates via the 'quantData' function, utilizing default parameters with the exception of data normalization, which was set to 'FALSE'. For plotting purposes, protein intensities were VSN normalized, log-transformed, and replicate batch effects were removed using the removeBatchEffect function in the limma R package. The limma package was also used to calculate differential protein expression. Multiple hypothesis correction was performed using the Benjamin Hochberg method.

Whole exome sequencing

Sample preparation

All cell lines were grown for several passages in the absence of antibiotics, gemcitabine or cisplatin. Cell pellets were snap frozen from sub-confluent dishes for each of the 20 cell lines sequenced (5 cell lines, each with 4 derivatives: parental, Gem-resistant, Cis-resistant, GemCis-resistant). gDNA isolation was performed using the Puregene cell and tissue kit (Qiagen) with the addition of RNase A Solution (Qiagen) according to manufacturer's instructions. gDNA was quantified using a Qubit 4.0, then sheared using a Covaris S220 Sonicator to 200bp. Libraries were constructed using the Sure Select All Exon v6 library kit (Agilent) following the XT library preparation workflow. Completed libraries were run on the 4200 Tape Station (Agilent) using D1000 screen tape. Libraries were quantitated using the Qubit, diluted to 4nM prior to verification of cluster efficiency using qPCR, then sequenced on the NovaSeq 6000 instrument (Illumina) (150bp, paired-end) at the University of Colorado Cancer Center Genomics Shared Resource. Mean insert size across all cell lines was 177.8 bp and mean coverage was 193.7X with > 96.8% at >30X. Individual call line quality control metrics are reported in **Table S12**.

Data processing

The analysis pipeline was developed using Nextflow. For the raw fastq files, Fastqc was used to assess overall quality. For computational efficiency, raw sequence reads were partitioned using BBMap (partition.sh) into 40 partitions. They then were aligned to the GRCh38 reference genome (including decoy sequences from the GATK resource bundle) using the BWA-MEM

short read aligner (Li, 2013), and merged back into single BAM files using Samtools. The resulting BAM files were de-duplicated using Samblaster (Faust and Hall, 2014), and sorted using Samtools. These duplicate-marked bams were further passed through the GATK Base Quality Score Recalibration in order to detect systematic errors made by the sequencing machine when it estimates the accuracy of base calls. The dbSNP (version 146) (Sherry et al., 2001), the 1000 Genome Project Phase 1 (1000 Genomes Project Consortium et al., 2015), and the Mills and 1000G gold standard sets (Mills et al., 2011) were used as databases of known polymorphic sites to exclude regions around known polymorphisms from analysis. After alignment, Samtools (Li et al., 2009), Qualimap (Okonechnikov et al., 2016), and Picard tools (2018) were run to acquire various metrics to ensure there were no major anomalies in the aligned data.

Alignment

bwa mem -K 100000000 -R "read_group" -t 64 -M ref_fasta read_1 read_2

Marking duplicates

samtools sort -n -O SAM sample_bam | samblaster -M --ignoreUnmated

Base Quality Score Recalibration

gatk BaseRecalibrator -I sample_bam -O sample.recal.table -R ref_fasta --known-sites known_sites

Whole exome sequencing variant calling

We used Mutect2 from the GATK toolkit for SNVs and short indels (Benjamin et al., 2019). Mutect2 is designed to call somatic variants and makes no assumptions about the ploidy of samples. It was run in *tumor-only* mode to maximize the sensitivity albeit at the risk of high false positives. We used tumor-only mode to call variants for each cell line separately. Mutect2 workflow is a two steps process. In the first step, it operates in high sensitivity mode to generate intermediate callsets that are further subjected to filtering to generate the final variant calls. Annotation of variants was performed using Annovar (Wang et al., 2010) with the following databases: refGene, cytoBand, exac03, avsnp150, clinvar_20190305, gnomad211_exome, dbnsfp35c, cosmic90. Intergenic variants were removed along with variants that were identified at greater than 0.001% of the population according to ExAC or gnomAD, or had a depth < 20.

Mutect2 raw callset:

gatk Mutect2 -R ref_fasta -I bam_tumor -tumor Id_tumor --germline-resource germline_resource -O raw_vcf

Mutect2 filtering:

gatk FilterMutectCalls -V raw_vcf --stats raw_vcf_stats -R ref_fasta -O filtered_mutect2_vcf

Copy number calling using GATK

Base quality score recalibrated bams were used as the input. The covered regions for the exome kit were converted into bins (defining the resolution of the analysis) for coverage collection. Read-counts, that form the basis of copy number variant detection, were collected for each bin. The read-counts then go through denoising, modelling segments, and calling the final copy ratios.

Preprocess intervals

gatk PreprocessIntervals --intervals intervals_bed_file --padding 0 --bin-length 0 -R ref_fasta --interval-merging-rule OVERLAPPING_ONLY -O preprocessed_intervals_list

Collect read counts

gatk CollectReadCounts -I sample_bam -L preprocessed_intervals} --interval-merging-rule OVERLAPPING_ONLY -O sample.counts.hdf5

Denoise read counts

gatk DenoiseReadCounts -I sample.counts.hdf5 --standardized-copy-ratios sample_std_copy_ratio --denoised-copy-ratios sample_denoised_copy_ratio

Model Segments

gatk ModelSegments --denoised-copy-ratios denoised_copy_ratio --output-prefix id_sample -O output_dir

Call copy ratio segments

gatk CallCopyRatioSegments -I sample.modelled_segments -O sampled.called.segments

Cell line authentication

Variant calls from the Mutect2 pipeline were filtered for each cell line to identify high confidence variants according to the filtering criteria above. These high confidence variants were then compared to the variants reported for all cell lines in the DepMap (https://depmap.org/portal/) for the Cancer Cell Line Encyclopedia (CCLE_mutations_hg38.csv, sample_info.csv) and COSMIC (CosmicCLP_MutantExport.tsv) as measured by the jaccard distance, the intersection of variants divided by the union of variants. Cells listed in CCLE or COSMIC were the rank ordered for each BCa cell line in this study according to the jaccard distance. Results are reported in **Table S13**.

Metabolomics

Sample preparation

Cell lines were cultured for several passages in IMDM + 10% FBS (IMDM10). Prior to experiment, cells were cultured in IMDM10 to ~80% confluence and then dissociated. For dissociation, cells were washed once with room temperature PBS and then incubated with PBS + 0.05% Trypsin-EDTA for 10-15 minutes. Cells were neutralized with IMDM10 and then fully dissociated by gentle pipetting. After dissociation, cells were counted by Trypan blue staining and then replated at 1e6 cells. 24 hours after plating, cells were treated with either IMDM10 or IMDM10 + 10μM cisplatin. Day 0 cell cultures were immediately processed for metabolomics analysis. To prepare cell pellets for metabolomics analysis, day 0 cells were dissociated and then centrifuged at 300RCF for 10 minutes at 4°C. Cells were suspended in PBS, centrifuged a second time, and then resuspended in PBS and counted. Day 0 cells were centrifuged a third time, the supernatants were aspirated, and the dry cell pellets were snap frozen in liquid nitrogen and stored at -80°C until metabolite extraction. 72 hours after plating, cells were processed for metabolomics analysis as described for the day 0 cell cultures.

Data generation and analysis

Metabolites from frozen cell pellets were extracted at 2e6 cells/mL in ice cold 5:3:2 MeOH:acetonitrile:water. Extractions were carried out using vigorous vortexing for 30 min at 4°C. Supernatants were clarified by centrifugation (10 min, 18,000 g, 4°C) and 10 μL analyzed using a Thermo Vanquish UHPLC coupled to a Thermo Q Exactive mass spectrometer. Global metabolomics analyses were performed using a 5 min C18 gradient in positive and negative ion modes (separate runs) with electrospray ionization as described in (Gehrke et al., 2019;

Nemkov et al., 2019). For all analyses, the MS scanned in MS^1 mode across the m/z range of 65 to 950. Peaks were annotated in conjunction with the KEGG database, integrated, and quality control performed using Maven as described in (Nemkov et al., 2015). Data was variance stabilization normalized (Huber et al., 2002), log2-transformed, and differential abundance calculations were done using limma (Ritchie et al., 2015) with time and/or treatment as covariates in the linear model.

Cell Line Drug Treatments

Gemcitabine (Sigma) and cisplatin (Sigma) stocks were resuspended in 0.9% saline solution and tosedostat (Sigma and BOC Sciences) was resuspended in DMSO. All stocks solutions were stored protected from light and kept frozen until use. For cell culture dose-response, cells were seeded in 96-well tissue culture plates with 500-2000 cells per well depending on growth rate and duration of experiment. Cells were seeded and allowed to attach overnight followed by replacing the media with fresh, pre-warmed media just prior to treatment. Drug dilutions were performed serially and using complete media (IMDM + 10% FBS) and the associated drug treatments. Growth inhibition was measured using confluence estimates over time on the IncuCyte ZOOM (Essen Bioscience, Ann Arbor, MI) over varying amounts of time depending on each experiment. Details for timing and replicates for each experiment are included in their respective figure legends.

Antibodies and Western Blotting

Whole cell lysates were prepared from cultured cells using RIPA lysis and extraction buffer (ThermoScientific). Lysates from xenograft tissues were prepared using tissue protein extraction reagent (T-PER) and glass tissue homogenizer. All lysates were prepared on ice and with the addition of Halt protease and phosphatase inhibitor cocktail and EDTA (ThermoFisher). Protein concentration of lysates were quatified with BCA protein assay (Pierce™, ThermoFisher). All lysates were prepared with 4X Licor Loading buffer with DTT added boiled for 10 minutes prior to gel loading. All western blots were run using PROTEAN TGX precast 4-15% or 4-20% gradient gels (Biorad) and transferred to either 0.2μm or 0.44μm nitrocellulose membranes. Transfer was done for 1.5-2hrs in cold TrisGlycine buffer (Biorad) with 20% methanol prior blocking for 1hr at room temperature in 5% BSA in TBS-T. Primary antibodies were diluted and incubated overnight at 4°C on a rocker. Membranes were washed 3 or 4 times in fresh TBS-T prior a 1 hour room temperature incubation in an appropriate secondary antibody. Membranes were washed 3-4 times in TBS-T, developed with enhanced SuperSignal West Pico Plus or SuperSignal West Fempto (ThermoFisher) and imaged using Li-Cor Odyssey® Fc instrument. Densitometry was performed using LiCor Image Studio™ software. Statistical comparisons using densitometry measurements were done using a one-way ANOVA with Tukey post hoc to control for the experimentwise error rate.

Cisplatin induced NPEPPS mRNA expression

Total RNA was isolated from cells and organoids using Trizol (ThermoFisher) and standard phenol-chloroform based extraction methods. Residual DNA was digested with DNAse I (Life technologies). cDNA synthesis was performed using Superscript II Reverse Transcriptase kit (Life technologies) using random primers. RT-qPCR reactions were performed on a CFX Connect Real-Time PCR Detection System thermocycler (Biorad) using TaqMan™ gene expression assays for NPEPPS and HMBS as a housekeeping gene (ThermoFisher) in combination with SensiFAST™ Probe No-ROX Kit (Bioline, Toronto, Canada). Expression data was calculated using $2^{-\Delta\Delta Ct}$. All cell line experiments were performed in triplicate from

independently grown cells. Comparisons were made between control treatment (0μM cisplatin) using a t-test.

siRNA-mediated knockdown experiments

NPEPPS and non-targeting siRNA smartpools were purchased from Horizon Discovery and resuspended in Dharmacon 5X siRNA Buffer. Transfections were performed using Lipofectamine RNAiMax (ThermoFisher) transfection reagent according to the manufacturer's specifications. Briefly, cells were grown to ~60% confluence in 6-well plates prior to being transfected and allowed to incubate overnight. The following day cells were trypsinized and replated into 96-well plates at 1000-2000 cells per well and allowed to attach overnight. Cells from the initial transfection were also replated into 6-well plates to collect protein and RNA to confirm knockdown. The following day, cells were treated using their previously established resistance doses of gemcitabine, cisplatin, or both (**Table S1**), and their relative growth rates were measured on the IncuCyte ZOOM (Essen Bioscience, Ann Arbor, MI) over time.

shRNA-mediated knockdown experiments

Lentiviral production and transduction were carried out by the University of Colorado Cancer Center Functional Genomics Shared Resources. Plasmids from The RNAi Consortium (TRC) collection (TRC construct numbers TRCN0000073838, TRCN0000073839 and TRCN0000073840) were used for targeting NPEPPS were selected based on predicted knockdown efficiency; non-targeting controls used were SHC002 and SHC016. 2μg of target shRNA construct and 2μg of 3:1 ratio of psPAX2 (Addgene) and pMD2.G (Addgene) were transfected into HEK293FT cells using 2 μg of Polyethylenimine (Polysciences, Inc.). Lentiviral particle containing media was filtered using 0.45μm cellulose acetate syringe filter and used for transduction. Puromycin selection was performed at doses used for CRISPR library screening or in some cases, cells were re-selected with higher doses of puromycin (10μg/mL), in order to ensure complete elimination of non-transduced cells. Selected cells were frozen at early passage and early passage cells were used for all experiments.

Intracellular cisplatin measurements using CyTOF

Cell lines were cultured for several passages in IMDM + 10% FBS. Prior to experiment, cells were cultured in IMDM10 to be 50-80% confluence overnight and then treated the next day with varying concentrations of cisplatin or PBS as indicated and then dissociated after 4 hours of treatment. For dissociation, cells were washed twice with room temperature PBS and then incubated with PBS + 0.05% Trypsin-EDTA for 10-15 minutes. Cells were neutralized with IMDM10 and then fully dissociated into single-cell suspension by gentle pipetting. After dissociation, cells were counted by Trypan blue staining and then placed in separate tubes at 3 x 10^5 cells. Individual samples were then fixed, permeabilized, and labeled using unique barcodes using the Cell-ID 20-plex Pd Barcoding kit (Fluidigm) according to the manufacturer protocol. Barcoded samples were pooled across cell line condition and cisplatin concentration, incubated with Cell-ID Intercalator-Ir, mixed with equilibration beads and acquired on a Helios mass cytometer (Fluidigm). Post-acquisition data were normalized to equilibration beads and debarcoded, using the bead-normalization and single-cell-debarcoder packages from the Nolan Laboratory GitHub page (https://github.com/nolanlab). Relative cisplatin intensity (defined by ^{195}Platinum isotopic mass intensity) was analyzed among nucleated ^{191}Iridium+ ^{193}Iridium+ events (defined by Boolean gating within FlowJo 10.7.1).

Whole Genome CRISPR Screening

Plasmid library expansion and quality control

Whole genome CRISPR Screening was performed using the Human CRISPR Knockout Pooled Library (Brunello) - 1 vector system (Addgene and a gift from John Doench to the Functional Genomics Facility at the University of Colorado Anschutz Medical Campus) (Doench et al., 2016b). Two distinct plasmid expansions were performed. And the library distribution was assessed using next generation sequencing to determine the impact on overall library was modest following re-expansion. Library width was calculated as previously described (Imkeller et al., 2020; Joung et al., 2017) by dividing the 10^{th} percentile of the library distribution by the 90^{th} percentile using the log2 average expression of all sgRNAs in the library and found to be 6.7 and 7.13 for batch 1 and 2 respectively. All quality control metrics for each sample are reported in **Table S14**. Different screening parameters were used based on the cell line screened these are summarized in **Table S4.**

Lentivirus Production and Titration

For the two plasmid batches, two distinct protocols for lentivirus production were utilized. The first batch was generated by using Polyethylenimine, linear (PEI; Polysciences Inc.) and the second using lipofectamine 3000. For the first batch, 293FT cells were seeded at a density of 36,800 cells/cm^2 into a 4-layer CELLdisc (Greiner) using DMEM + 10% FBS along with Antibiotic and antimycotic solution. Transfection mix consisting 47.6μg pMD2G (Addgene), 95.2μg of psPAX2 (Addgene), and 190.5μg of Brunello Whole genome knockout library (Addgene) was mixed with 448μl PEI (1 mg/mL) and 3mL OptiMEM, vortexed for 30 seconds and allowed to incubate at room temperature for 20 minutes. Fresh media containing transfection mix were added to the CELLdisc using up to 270mL of media. The next day media was changed for 280mL fresh media followed by a 48 hour incubation. After this 48 hour incubation the viral supernatant was harvested and filtered through a cellulose acetate filter system (ThermoScientific) and frozen at -80°C.

The first method had low functional virus titer, so we attempted a different virus production method for subsequent screens. In the second batch of virus production we utilized lipofectamine 3000 instead of PEI, eliminated use of multilayer flasks and centrifuged to remove debris as opposed to filtering. Briefly, 293FT cells were plated in T225 flasks to be 80% confluent after 24hrs. 2hrs before transfection, media was changed and 40mL of fresh media was used per T225 flask. The lipofectamine 3000 protocol was followed according to manufacturer's instructions and scaled based on the volume of virus being prepared. For each T225 flask 2mLOptiMEM was mixed with 40μg Brunello whole genome library plasmid, 30μg of psPAX2 and 20μg of pMD2.G and 180μl of P3000. This mix was added to a tube containing 2mL OptiMEM and 128μl Lipofectamine 3000, which was scaled according to the number of T225 flasks being prepared. Transfection mix was mixed thoroughly by pipetting up and down slowly, and allowed to incubate at room temperature for 15 minutes. Transfection mix was then added dropwise to the plates of 293FT cells with gentle swirling and incubated overnight (~16hr). The following morning, the media was changed and 60mL of fresh media was added to each T225 flask. This was allowed to incubate overnight and replaced the following morning. This first lentiviral supernatant was stored at 4°C to be pooled with a subsequent 48 hour collection. Upon collection, viral supernatants had 1M HEPES added at 1%. Following the second virus collection, supernatants were pooled and centrifuged at 1250rpm for 5 minutes to pellet debris. Lentivirus was stored in polypropylene tubes as polystyrene is known to bind lentivirus, and all tubes were flash frozen in liquid nitrogen and stored at -80°C. Despite the

changes to the lentiviral production protocols, functional lentiviral titers were not improved using these changes to the methodology, but feel it is worth noting these changes in protocol to account for any possible variability associated with this change.

Lentivirus was titered functionally based on protocols adapted from the Broad Institute's Genetic Pertubation Platform's public web portal (https://portals.broadinstitute.org/gpp/public/).

Screening Parameter Optimization

All screening parameters for each cell lines including cell polybrene and puromycin sensitivity, screening coverage, technical and biological replicates performed, and gemcitabine and cisplatin treatment concentrations are reported in **Table S4.**

DNA Isolation

Cell pellets of $2.0X10^7$ were snap frozen in liquid nitrogen in 1.5mL tubes and stored at -80 prior to extraction. When possible at least $8.0X10^7$ cell were used for 4 separate genomic DNA isolation which were pooled to account for any variation with pellet size. DNA isolation was performed using the Puregene cell and tissue kit (Qiagen) with the addition of RNase A Solution (Qiagen) according to manufacturer's instructions. DNA concentration was measured in quadruplicate using either a nanodrop spectrophotometer (Thermo), Qubit® dsDNA assay (Life Technologies) and the average DNA content per cell was determined.

Library preparation

The minimum number of cell equivalents of gDNA to maintain equal coverage was used for library preparation. In all screens, the minimum coverage based on cell number was multiplied by the average gDNA content per cell for each individual cell line to determine the minimum number for 10μg PCR reactions needed to maintain coverage. A minimum coverage of 500-fold per sgRNA in the library was targeted for each independent sample or replicate but this was increased in some cases where screening was carried out with greater depth (see **Table S4** for coverage and replicate information).

Library preparation was performed using primers sequences designed by the Broad Institute's Genetic Perturbation Platform (https://portals.broadinstitute.org/gpp/public/) and utilized a pool of eight P5 primers with to introduce a stagger in reads associated with each library and sample specific P7 primer that contained a unique sample index sequence for each timepoint, replicate, or treatment condition to be sequenced in the same pool (**Table S11**). All library preparation primers were resuspended at 100μM.

Each library preparation PCR reaction contained the following components: 1μl Herculase II Fusion Enzyme (Agilent), 2.5μl Deoxynucleotide (dNTP) Solution Mix (New England Biolabs), 0.5μl P5 primer pool, 0.5μl P7 index primer, 20μl 5X Reaction Buffer (Agilent), 10μg of gDNA and nuclease-free water to bring the total reaction volume to 100μl. Samples underwent 23 cycles of thermal cycling followed by a quality assessment by electrophoresis on 2% agarose gel to ensure consistent library amplification across multiple wells and samples for each plate.

Each unique library had 10μl pooled from all PCR reactions performed on that unique sample and mixed thoroughly. 50-100μl of the pooled library preparation reactions was used to perform magnetic bead-based purification and elimination of any residual free primer using a 0.8X ratio SPRIselect beads (Beckman Coulter) according to the manufacturer's instructions. Libraries were then assessed for appropriate amplicon size and complete elimination of free primer peaks using the High Sensitivity ScreenTape Assay on the Tape Station2200 (Agilent) and quantified using the qPCR-based quantification in order to ensure only NGS-compatible amplicon was quantified using the Library Quant ROX Low Kit (Kapa Biosystems) on a QuantStudio™ 6

Realtime PCR System (ThermoFisher). Following qPCR quantification, all libraries were normalized to a standard concentration (typically 20-40nM) depending on the lowest concentration library to be pooled, and then requantified by qPCR to ensure all samples were within ~10-20% of the pool mean target concentration. After confirming accurate library quantification and normalization, samples were pooled at an equimolar ratio and submitted for sequencing. Libraries were sequenced on the NovaSeq 6000 instrument (Illumina) (150bp, paired-end) at the University of Colorado Cancer Center Genomics Shared Resource.

CRISPR screening bioinformatic pipeline and analysis

sgRNA counts were extracted directly from R1 raw sequence reads using a custom perl script that uses regular expression string matching to exactly match sgRNA sequence flanked by 10 bases of vector sequence. The vector sequence was allowed to have one error before and after the sgRNA sequence. sgRNAs were tabulated for each sample based on the sgRNA sequence (**Table S15**). The sgRNA IDs of the Brunello library were updated to current HGNC gene names using the Total Approved Symbols download from HGNC, accessed on 9/1/2020 (https://www.genenames.org/download/statistics-and-files/). Transcript IDs were matched when possible and when matches were not found, past symbols and aliases were updated to current names. Finally, 5 sgRNAs with missing updated gene names were manually curated using literature searches. Library distribution was calculated using the caRpools R package (Winter et al., 2016) (**Table S11)**. The DESeq2 R package (Love et al., 2014) was used to calculate differential abundance of genes (**Table S5**). Gene counts were generated using the sum of counts for sgRNAs of the same gene. Synthetic Lethality compared GemCis day 19 and GemCis day 25 vs. Saline day 19 and Saline day 25 with the day as a covariate. In the comparison integrating all cell lines, cell line was additionally modeled as a covariate. Gene essentiality was calculated by comparing Saline day 25 to Saline day 0 and in the integrated all cell lines comparison, cell line was modeled as a covariate. Common synthetic lethal genes were defined as being statistically significantly differentially lost (FDR < 0.05 and Log2 FC < 0) in each of the 5 cell lines. Gene set enrichment analysis (GSEA) was performed using the fgsea R package run with 10000 permutations (Sergushichev, 2016) with the KEGG and Reactome gene sets from MSigDB (Liberzon et al., 2011). Heatmaps were generated with the ComplexHeatmap R package following z-score transformation (Gu et al., 2016). Other plots were generated using the ggplot2 R package.

Xenograft experiments

Six-week-old, female Nu/J mice (Jackson Labs) were allowed to acclimate for at least one week prior to initiating any experiments. Mice had free access to food and water in pathogen-free housing and cared for in accordance NIH guidelines and all experiments were performed under protocols approved by the University of Colorado Denver Institutional Animal Care and Use Committee (IACUC).

For KU1919-GC xenografts, cells that had been stably transduced with non-targeting control (shCtrl1, SHC002) and NPEPPS (shN39, TRCN0000073839) shRNA constructs. Mice were divided into groups of 22 and 23 for the non-targeting control and NPEPPS shRNA constructs respectively. Mice were injected with $4X10^6$ cells in phenol red- and serum-free RPMI mixed with equal volume Matrigel Matrix (Corning) to total 100μl volume. Tumors were allowed to engraft for 9 days following injection and mice were randomized based on tumor volume within each shRNA condition into groups of 11 or 12 to be treated with combination gemcitabine plus cisplatin or DPBS. Treatment was initiated 13 days post-inoculation with dosing adjusted based on individual mouse weight.

Cisplatin (Sigma) and gemcitabine hydrochloride (BOC Sciences) were both resuspended in 0.9% saline and stored protected from light at -80°C as individual aliquots. Prior to treatment

fresh aliquots of gemcitabine and cisplatin were thawed and diluted to their final concentration with 1X DPBS (Gibco). Mice were treated three times weekly on a Monday, Wednesday and Friday schedule for four weeks total. All mice in the gemcitabine plus cisplatin treated groups were given 50mg/kg gemcitabine and 2mg/kg cisplatin that were mixed and administered as a single intraperitoneal injection, while control mice were administered an equivalent volume of DPBS.

Mouse health was monitored daily and all tumor volume measurements and weights were measured 3x weekly schedule. Tumor volume was calculated using the formula (L x W^2)/2, for which L *is* the length of the long axis and W is the width of the axis perpendicular to the long axis measurement. All measurements were performed using digital calipers. Animal were humanely euthanized with CO_2 followed by cervical dislocation when tumors reached a predetermined endpoint of 2cm^3 or when weight loss exceeded 15% body weight. Mice that were removed from study due to weight loss were censored in the survival analyses.

Linear mixed-effects model of tumor growth

Linear mixed-effects models were used to model longitudinal observations of xenograft tumor growth volumes normalized by their corresponding baseline volume. Mixed-effects models from the R-package *lme4* (Bates et al., 2015) and Satterthwaite's approximation for degrees of freedom for the fixed effects from *lmerTest* (Kuznetsova et al., 2017) were used for model fitting and inspection in the R statistical software (4.0.3). Volume changes compared to baseline were $\log_2$-transformed. The final model was structured as:

$$log_2\left(\frac{y_{i,t}}{y_{i,:}}\right) = \beta_0 + \beta_1 x_{i,t} + \beta_2 x_{i,t}^2 + \beta_3 x_{i,t} KD_i + \beta_4 x_{i,t} GC_i + \beta_5 x_{i,t} KD_i\, GC_i + \gamma_{0,i} + \gamma_{1,i} x_{i,t} + \varepsilon_{i,t}$$

where β is the fixed effects capturing population-level trends, γ is the normally distributed random effects capturing individual-level variation, ε is the i.i.d. normally distributed residual term, i is the unique individual identifier, t notes the time points, $x_{i,t} \in \{2, 4, 5, 7, 9, 11, 14, 16, 18, 21, 23, 25, 28\}$ depicted days since initiating interventions, $y_{i,:}$ is tumour volume at baseline prior to treatments upon randomization, and $y_{i,t}$ were the observed tumour volumes over the treatment period measured in mm^3. The model was fit using Restricted Maximum Likelihood and built iteratively until the underlying model assumptions and model convergence criteria were met. To this end, a quadratic growth term (β_2) was added on top of the linear growth term (β_1) and intercept (β_0), allowing slightly non-linear relative growth patterns to be captured by the otherwise linear model. Binary indicators $KD_i \in \{0,1\}$ and $GC_i \in \{0,1\}$ were used to model knockdown of NPEPPS (KD), GemCis therapy (GC), or both combined. The corresponding model terms were captured in β_3, β_4 and β_5, respectively. Finally, the model allows for individual-specific random effects for intercept ($\gamma_{0,i}$) and linear growth slope ($\gamma_{1,i}$). Shapiro-Wilk test was used to examine the underlying normality assumption for $\gamma_{0,i}$ and $\gamma_{1,i}$ with p=0.1373 and p=8901, respectively, indicating that these random effects followed underlying assumptions of normality. After inspection of the residual plots (**Figure S9B**), this final model was deemed suitable for population-level statistical inference via the fixed effects. This population-level model fits are visualized in **Figure S9A**. These population-level estimates are as follows:

Fixed effect	**Estimate**	**Std. error**	**df**	**t**	***p*-val**
β_0 (intercept)	0.05054	0.08422	54.28	0.600	0.55091
β_1 (linear slope)	0.1236	0.01493	65.52	8.276	8.92e-12 ***
β_2 (quadratic slope)	0.00308	0.0002242	389	13.740	< 2e-16 ***
β_3 (knockdown)	-0.0605	0.01821	44.97	-3.322	0.00178 **
β_4 (GC)	-0.1063	0.01821	44.97	-5.837	5.49e-07 ***

β_5 (knockdown + GC)	-0.1233	0.01791	45.28	-6.884	1.47e-08 ***

Survival analyses from TCGA

Copy number and gene expression data for patients with muscle-invasive bladder cancer in the TCGA cohort (PanCancer Atlas) were downloaded from cBioPortal (Cerami et al., 2012; Gao et al., 2013). Patient survival and platinum-based treatment annotation was from our previous work (Goodspeed et al., 2019). Patients were separated into treatment groups, platinum-based treatment (n = 100) or unrecorded treatment (n = 204), and then stratified based on copy number gain or amplification, or mRNA upregulation (z-score > 1) of LRRC8A or LRRC8D. The Logrank test was used to test the difference in overall survival between the stratified patient groups.

Tumor-derived Organoids

Culture of the organoids

Human bladder tissue was obtained from the Erasmus MC Bladder Cancer Center, Rotterdam, the Netherlands. Bladder tumor-derived organoids from biopsies obtained through TURBT or cystectomy were isolated and cultured using a method based on (Mullenders et al., 2019) with modifications (Akbarzadeh/Scholtes et al. in prep). Briefly, Bladder tissues were washed with Advanced DMEM/F12 (Gibco) supplemented with 10mM HEPES (Gibco), 1% GlutaMax (Gibco) and 100 µg/ml primocin (InvivoGen), henceforth Ad+++. Tissue was minced and incubated at 37°C with the digestion solution (collagenase 2.5mg/ml in EBSS) and isolated cells were passed through 70µM strainer (Falcon), washed with Ad+++ and seeded in 50 µl drops of BME (R&D system) containing 10000-15000 cells in 24 well suspension plates (Greiner). Bladder tumor organoids were cultured in a culture medium containing Ad+++ supplemented with 1 × B-27 (Gibco), 1.25 mM N-acetylcysteine (Sigma), 10 mM nicotinamide, 20µM TGFβ receptor inhibitor A83-01, 100ng/ml recombinant human FGF10 (Peprotech), 25 ng/ml recombinant human FGF7 (Peprotech), 12.5 ng/ml recombinant human FGF2 (Peprotech), 10µM Y27632 Rho Kinase (ROCK) Inhibitor (Sigma) and conditioned media for recombinant Rspondin (2.5% v/v), and Wnt3A (2.5% v/v). The medium was changed every three days. Organoids were passaged at a 1:3 to 1:6 ratio every 7 days using cell dissociation solution- non enzymatic (Sigma) and plated in fresh BME matrix droplets.

Drug screening

Organoids were collected 7 days after passaging, passed through a 100µM strainer and 1000 organoids were seeded per well of a 48-well plate in BME matrix droplets. After 24h, cisplatin (Sigma) resuspended in PBS was added at different concentrations (2, 10, 25, and 50 µM) with or without tosedostat (20 µM) (Tocris) resuspended in DMSO. Organoids were cultured for the first 6 days in the presence of drugs followed by drug withdrawal, where organoids were grown in organoid culture media for 10 days. The entire content of the wells in different treatment groups was collected, washed and reseeded after disaggregation in fresh BME, and cultured for 6 days. Cell viability was assayed using alamarBlue (Invitrogen) according to the manufacturer's instructions after 6 days of drug incubation, 10 days of drug withdrawal, and 6 days post reseeding. Viability data was normalized using organoid wells treated with vehicle control.

SNaPshot mutation and microarray analysis

Tumor, organoid, and matched normal DNA was isolated using with the QIAmp DNA Mini-Kit (Qiagen) according to the manufacturer's protocol. Presence of hotspot mutations in the *TERT* promoter sequence chr5:1,295,228C>T, chr5:1,295,248G>A and chr5:1,295,250C>T [GRCh37/hg19]), *FGFR3* (R248Q/E, S249C, G372C, Y375C, A393E, K652E/M) and *PIK3CA*

(E542K, E545G/K and H1047R) were assessed on tumor, normal and organoid DNA by SNaPshot mutation analysis with the same methods as previously described (Allory et al., 2014; Hurst et al., 2009; Junker et al., 2008). Copy number aberration analysis was performed using single-nucleotide polymorphism (SNP) microarrays (Affymetrix GSA V3, Affymetrix) on primary tumor DNA, matched DNA collected from normal urothelium plus stromal tissue from the same sample but from a distant location from the tumor, and organoid DNA using standard protocols. SNP data (log-R ratio, B-allele frequency) were visualized to identify potential CNVs via Biodiscovery Nexus CN7.5. (Biodiscovery) and the GenomeStudio genotyping module (Illumina).

Organoid phenotyping and tumor histology

Tissue processing and H&E staining was performed using standard procedures. For hematoxylin-eosin (H&E) staining of organoids, wells of BME-embedded organoids were fixated with 4% formalin (Sigma) and 0.15% glutaraldehyde (produced in-house) at room temperature for 2 hours. Fixated BME and organoids were washed with PBS and engulfed in 2.5% Low-Melting Agarose (Sigma) prior to paraffin embedding. H&E staining was performed on 4µM paraffin sections of both tumor and organoid tissue. Stained whole-slides, as well as prior 3D organoid cultures were imaged by bright-field microscopy (Olympus IX70).

Acknowledgements

We would like to thank Megan Tu, Colin Sempeck, Ana Chauca-Diaz, Jason Duex, and Charles Owens for their help throughout this project. This work was generously supported by the Anschutz Foundation to J.C.C., CA180175 to D.T., FICAN Cancer Researcher by the Finnish Cancer Institute to T.D.L., Erasmus MC mRACE grant 111296 to T.M. and T.Z., Erasmus MC fellowship project 107088 to T.Z., and training grants GM007635 and GM008497 supported R.T.J. This work utilized the Functional Genomics Facility, Biostatistics and Bioinformatics Shared Resource, Genomics Shared Resource, and Flow Cytometry Shared Resource supported by CA046934.

Author Contributions

Conceptualization: R.T.J., T.M., T.Z., D.T., J.C.C.
Methodology: R.T.J., A.G., M.S., H.V., A.J., T.D.L., M.A., E.C., S.P., T.M., T.Z., D.T., J.C.C.
Software: A.G., T.D.L., M.J., R.L., J.C.C.
Validation: R.T.J., A.G., M.S., A.J., C.T., M.V.O., T.Z.
Formal Analysis: R.T.J., A.G., M.S., H.V., T.D.L., M.V.O., M.J., E.C., S.P., T.Z., D.T., J.C.C.
Investigation: R.T.J., M.A., M.S., H.V., A.J., C.T., M.V.O., E.C., S.P., T.Z., J.C.C.
Resources: A.J., C.T., E.C., R.L., T.Z.
Data Curation: R.T.J., A.G., A.J., T.D.L., M.J., R.L., J.C.C.
Writing – Orginal Draft: R.T.J., A.G., D.T., J.C.C.
Writing – Review & Editing: R.T.J., A.G., M.A., M.S., H.V., M.V.O., M.J., T.D.L., E.C., S.P., T.M., T.Z., D.T., J.C.C.
Visualization: R.T.J., A.G., M.A., M.S., M.V.O., T.D.L., E.C., T.Z., D.T., J.C.C.
Supervision: R.L., T.M., D.T., T.Z., J.C.C.
Project Administration: R.T.J., A.J., T.M., T.Z., D.T., J.C.C.
Funding Acquisition: T.M., T.Z., D.T, J.C.C.

Declaration of Interests

J.C.C. is co-founder of PrecisionProfile.

References

1000 Genomes Project Consortium, Auton, A., Brooks, L.D., Durbin, R.M., Garrison, E.P., Kang, H.M., Korbel, J.O., Marchini, J.L., McCarthy, S., McVean, G.A., et al. (2015). A global reference for human genetic variation. Nature *526*, 68–74.

Allory, Y., Beukers, W., Sagrera, A., Flández, M., Marqués, M., Márquez, M., van der Keur, K.A., Dyrskjot, L., Lurkin, I., Vermeij, M., et al. (2014). Telomerase reverse transcriptase promoter mutations in bladder cancer: high frequency across stages, detection in urine, and lack of association with outcome. Eur. Urol. *65*, 360–366.

Balar, A.V., Galsky, M.D., Rosenberg, J.E., Powles, T., Petrylak, D.P., Bellmunt, J., Loriot, Y., Necchi, A., Hoffman-Censits, J., Perez-Gracia, J.L., et al. (2017a). Atezolizumab as first-line treatment in cisplatin-ineligible patients with locally advanced and metastatic urothelial carcinoma: a single-arm, multicentre, phase 2 trial. Lancet Lond. Engl. *389*, 67–76.

Balar, A.V., Castellano, D., O'Donnell, P.H., Grivas, P., Vuky, J., Powles, T., Plimack, E.R., Hahn, N.M., de Wit, R., Pang, L., et al. (2017b). First-line pembrolizumab in cisplatin-ineligible patients with locally advanced and unresectable or metastatic urothelial cancer (KEYNOTE-052): a multicentre, single-arm, phase 2 study. Lancet Oncol. *18*, 1483–1492.

Bates, D., Mächler, M., Bolker, B., and Walker, S. (2015). Fitting Linear Mixed-Effects Models Using lme4. J. Stat. Softw. *67*, 1–48.

Behan, F.M., Iorio, F., Picco, G., Gonçalves, E., Beaver, C.M., Migliardi, G., Santos, R., Rao, Y., Sassi, F., Pinnelli, M., et al. (2019). Prioritization of cancer therapeutic targets using CRISPR–Cas9 screens. Nature *568*, 511–516.

Benjamin, D., Sato, T., Cibulskis, K., Getz, G., Stewart, C., and Lichtenstein, L. (2019). Calling Somatic SNVs and Indels with Mutect2. BioRxiv 861054.

Bepler, G., Kusmartseva, I., Sharma, S., Gautam, A., Cantor, A., Sharma, A., and Simon, G. (2006). RRM1 modulated in vitro and in vivo efficacy of gemcitabine and platinum in non-small-cell lung cancer. J. Clin. Oncol. Off. J. Am. Soc. Clin. Oncol. *24*, 4731–4737.

Bergman, A.M., Eijk, P.P., Ruiz van Haperen, V.W.T., Smid, K., Veerman, G., Hubeek, I., van den Ijssel, P., Ylstra, B., and Peters, G.J. (2005). In vivo induction of resistance to gemcitabine results in increased expression of ribonucleotide reductase subunit M1 as the major determinant. Cancer Res. *65*, 9510–9516.

Berle, M., Ghila, L., Vethe, H., Chaudhry, A., Garberg, H., Beisland, C., Haaland, Ø.A., Oveland, E., Halvorsen, O.J., Davidsson, T., et al. (2018). Novel protein signatures suggest progression to muscular invasiveness in bladder cancer. PloS One *13*, e0206475.

Bray, F., Ferlay, J., Soerjomataram, I., Siegel, R.L., Torre, L.A., and Jemal, A. (2018). Global cancer statistics 2018: GLOBOCAN estimates of incidence and mortality worldwide for 36 cancers in 185 countries. CA. Cancer J. Clin. *68*, 394–424.

Cerami, E., Gao, J., Dogrusoz, U., Gross, B.E., Sumer, S.O., Aksoy, B.A., Jacobsen, A., Byrne, C.J., Heuer, M.L., Larsson, E., et al. (2012). The cBio Cancer Genomics Portal: An Open Platform for Exploring Multidimensional Cancer Genomics Data. Cancer Discov. *2*, 401–404.

Chang, Q., Ornatsky, O.I., Koch, C.J., Chaudary, N., Marie-Egyptienne, D.T., Hill, R.P., Tanner, S.D., and Hedley, D.W. (2015). Single-cell measurement of the uptake, intratumoral distribution and cell cycle effects of cisplatin using mass cytometry. Int. J. Cancer *136*, 1202–1209.

Choi, M., Chang, C.-Y., Clough, T., Broudy, D., Killeen, T., MacLean, B., and Vitek, O. (2014). MSstats: an R package for statistical analysis of quantitative mass spectrometry-based proteomic experiments. Bioinforma. Oxf. Engl. *30*, 2524–2526.

Clasquin, M.F., Melamud, E., and Rabinowitz, J.D. (2012). LC-MS data processing with MAVEN: a metabolomic analysis and visualization engine. Curr. Protoc. Bioinforma. *Chapter 14*, Unit14.11.

Compagnone, M., Cifaldi, L., and Fruci, D. (2019). Regulation of ERAP1 and ERAP2 genes and their disfunction in human cancer. Hum. Immunol. *80*, 318–324.

Constam, D.B., Tobler, A.R., Rensing-Ehl, A., Kemler, I., Hersh, L.B., and Fontana, A. (1995). Puromycin-sensitive aminopeptidase. Sequence analysis, expression, and functional characterization. J. Biol. Chem. *270*, 26931–26939.

Cortes, J., Feldman, E., Yee, K., Rizzieri, D., Advani, A.S., Charman, A., Spruyt, R., Toal, M., and Kantarjian, H. (2013). Two dosing regimens of tosedostat in elderly patients with relapsed or refractory acute myeloid leukaemia (OPAL): a randomised open-label phase 2 study. Lancet Oncol. *14*, 354–362.

Cowley, G.S., Weir, B.A., Vazquez, F., Tamayo, P., Scott, J.A., Rusin, S., East-Seletsky, A., Ali, L.D., Gerath, W.F., Pantel, S.E., et al. (2014). Parallel genome-scale loss of function screens in 216 cancer cell lines for the identification of context-specific genetic dependencies. Sci. Data *1*, 140035.

Dempster, J.M., Krill-Burger, J., Warren, A., McFarland, J.M., Golub, T.R., and Tsherniak, A. (2020). Gene expression has more power for predicting in vitro cancer cell vulnerabilities than genomics. BioRxiv 2020.02.21.959627.

Dilruba, S., and Kalayda, G.V. (2016). Platinum-based drugs: past, present and future. Cancer Chemother. Pharmacol. *77*, 1103–1124.

Dobin, A., Davis, C.A., Schlesinger, F., Drenkow, J., Zaleski, C., Jha, S., Batut, P., Chaisson, M., and Gingeras, T.R. (2013). STAR: ultrafast universal RNA-seq aligner. Bioinforma. Oxf. Engl. *29*, 15–21.

1207 Doench, J.G., Fusi, N., Sullender, M., Hegde, M., Vaimberg, E.W., Donovan, K.F., Smith, I.,
1208 Tothova, Z., Wilen, C., Orchard, R., et al. (2016a). Optimized sgRNA design to maximize activity
1209 and minimize off-target effects of CRISPR-Cas9. Nat. Biotechnol. *34*, 184–191.

1210 Doench, J.G., Fusi, N., Sullender, M., Hegde, M., Vaimberg, E.W., Donovan, K.F., Smith, I.,
1211 Tothova, Z., Wilen, C., Orchard, R., et al. (2016b). Optimized sgRNA design to maximize activity
1212 and minimize off-target effects of CRISPR-Cas9. Nat. Biotechnol. *34*, 184–191.

1213 Drayton, R.M., and Catto, J.W. (2012). Molecular mechanisms of cisplatin resistance in bladder
1214 cancer. Expert Rev. Anticancer Ther. *12*, 271–281.

1215 Drinkwater, N., Lee, J., Yang, W., Malcolm, T.R., and McGowan, S. (2017). M1 aminopeptidases
1216 as drug targets: broad applications or therapeutic niche? FEBS J. *284*, 1473–1488.

1217 Faust, G.G., and Hall, I.M. (2014). SAMBLASTER: fast duplicate marking and structural variant
1218 read extraction. Bioinforma. Oxf. Engl. *30*, 2503–2505.

1219 FlowJo (2019). FlowJo Software (for Mac) (Becton, Dickenson and Company).

1220 Galluzzi, L., Senovilla, L., Vitale, I., Michels, J., Martins, I., Kepp, O., Castedo, M., and Kroemer,
1221 G. (2012). Molecular mechanisms of cisplatin resistance. Oncogene *31*, 1869–1883.

1222 Galsky, M.D., Pal, S.K., Lin, S.-W., Ogale, S., Zivkovic, M., Simpson, J., Derleth, C., Schiff, C., and
1223 Sonpavde, G. (2018). Real-World Effectiveness of Chemotherapy in Elderly Patients With
1224 Metastatic Bladder Cancer in the United States. Bladder Cancer Amst. Neth. *4*, 227–238.

1225 Galsky, M.D., Arija, J.Á.A., Bamias, A., Davis, I.D., De Santis, M., Kikuchi, E., Garcia-Del-Muro, X.,
1226 De Giorgi, U., Mencinger, M., Izumi, K., et al. (2020). Atezolizumab with or without
1227 chemotherapy in metastatic urothelial cancer (IMvigor130): a multicentre, randomised,
1228 placebo-controlled phase 3 trial. Lancet Lond. Engl. *395*, 1547–1557.

1229 Gao, J., Aksoy, B.A., Dogrusoz, U., Dresdner, G., Gross, B., Sumer, S.O., Sun, Y., Jacobsen, A.,
1230 Sinha, R., Larsson, E., et al. (2013). Integrative Analysis of Complex Cancer Genomics and Clinical
1231 Profiles Using the cBioPortal. Sci. Signal. *6*, pl1–pl1.

1232 Gehrke, S., Rice, S., Stefanoni, D., Wilkerson, R.B., Nemkov, T., Reisz, J.A., Hansen, K.C., Lucas,
1233 A., Cabrales, P., Drew, K., et al. (2019). Red Blood Cell Metabolic Responses to Torpor and
1234 Arousal in the Hibernator Arctic Ground Squirrel. J. Proteome Res. *18*, 1827–1841.

1235 Goodspeed, A., Jean, A., and Costello, J.C. (2019). A Whole-genome CRISPR Screen Identifies a
1236 Role of MSH2 in Cisplatin-mediated Cell Death in Muscle-invasive Bladder Cancer. Eur. Urol. *75*,
1237 242–250.

1238 Grossman, H.B., Natale, R.B., Tangen, C.M., Speights, V.O., Vogelzang, N.J., Trump, D.L., White,
1239 R.W. deVere, Sarosdy, M.F., Wood, D.P., Raghavan, D., et al. (2003). Neoadjuvant

1240 Chemotherapy plus Cystectomy Compared with Cystectomy Alone for Locally Advanced Bladder
1241 Cancer. N. Engl. J. Med. *349*, 859–866.

1242 Gu, Z., Eils, R., and Schlesner, M. (2016). Complex heatmaps reveal patterns and correlations in
1243 multidimensional genomic data. Bioinformatics *32*, 2847–2849.

1244 van Herpen, C.M.L., Eskens, F. a. L.M., de Jonge, M., Desar, I., Hooftman, L., Bone, E.A., Timmer-
1245 Bonte, J.N.H., and Verweij, J. (2010). A Phase Ib dose-escalation study to evaluate safety and
1246 tolerability of the addition of the aminopeptidase inhibitor tosedostat (CHR-2797) to paclitaxel
1247 in patients with advanced solid tumours. Br. J. Cancer *103*, 1362–1368.

1248 Hitzerd, S.M., Verbrugge, S.E., Ossenkoppele, G., Jansen, G., and Peters, G.J. (2014). Positioning
1249 of aminopeptidase inhibitors in next generation cancer therapy. Amino Acids *46*, 793–808.

1250 Huang, A., Garraway, L.A., Ashworth, A., and Weber, B. (2020). Synthetic lethality as an engine
1251 for cancer drug target discovery. Nat. Rev. Drug Discov. *19*, 23–38.

1252 Huber, W., von Heydebreck, A., Sültmann, H., Poustka, A., and Vingron, M. (2002). Variance
1253 stabilization applied to microarray data calibration and to the quantification of differential
1254 expression. Bioinforma. Oxf. Engl. *18 Suppl 1*, S96-104.

1255 Hurst, C.D., Zuiverloon, T.C.M., Hafner, C., Zwarthoff, E.C., and Knowles, M.A. (2009). A
1256 SNaPshot assay for the rapid and simple detection of four common hotspot codon mutations in
1257 the PIK3CA gene. BMC Res. Notes *2*, 66.

1258 Huttlin, E.L., Bruckner, R.J., Navarrete-Perea, J., Cannon, J.R., Baltier, K., Gebreab, F., Gygi, M.P.,
1259 Thornock, A., Zarraga, G., Tam, S., et al. (2020). Dual Proteome-scale Networks Reveal Cell-
1260 specific Remodeling of the Human Interactome. BioRxiv 2020.01.19.905109.

1261 Imkeller, K., Ambrosi, G., Boutros, M., and Huber, W. (2020). gscreend: modelling asymmetric
1262 count ratios in CRISPR screens to decrease experiment size and improve phenotype detection.
1263 Genome Biol. *21*, 53.

1264 Jordheim, L.P., Sève, P., Trédan, O., and Dumontet, C. (2011). The ribonucleotide reductase
1265 large subunit (RRM1) as a predictive factor in patients with cancer. Lancet Oncol. *12*, 693–702.

1266 Jost, M., and Weissman, J.S. (2018). CRISPR Approaches to Small Molecule Target Identification.
1267 ACS Chem. Biol. *13*, 366–375.

1268 Joung, J., Konermann, S., Gootenberg, J.S., Abudayyeh, O.O., Platt, R.J., Brigham, M.D., Sanjana,
1269 N.E., and Zhang, F. (2017). Genome-scale CRISPR-Cas9 knockout and transcriptional activation
1270 screening. Nat. Protoc. *12*, 828–863.

1271 Junker, K., van Oers, J.M.M., Zwarthoff, E.C., Kania, I., Schubert, J., and Hartmann, A. (2008).
1272 Fibroblast growth factor receptor 3 mutations in bladder tumors correlate with low frequency
1273 of chromosome alterations. Neoplasia N. Y. N *10*, 1–7.

1274 Karczewski, K.J., Francioli, L.C., Tiao, G., Cummings, B.B., Alföldi, J., Wang, Q., Collins, R.L.,
1275 Laricchia, K.M., Ganna, A., Birnbaum, D.P., et al. (2020). The mutational constraint spectrum
1276 quantified from variation in 141,456 humans. Nature *581*, 434–443.

1277 Karsten, S.L., Sang, T.-K., Gehman, L.T., Chatterjee, S., Liu, J., Lawless, G.M., Sengupta, S., Berry,
1278 R.W., Pomakian, J., Oh, H.S., et al. (2006). A genomic screen for modifiers of tauopathy
1279 identifies puromycin-sensitive aminopeptidase as an inhibitor of tau-induced
1280 neurodegeneration. Neuron *51*, 549–560.

1281 Kasuya, G., Nakane, T., Yokoyama, T., Jia, Y., Inoue, M., Watanabe, K., Nakamura, R., Nishizawa,
1282 T., Kusakizako, T., Tsutsumi, A., et al. (2018). Cryo-EM structures of the human volume-
1283 regulated anion channel LRRC8. Nat. Struct. Mol. Biol. *25*, 797–804.

1284 Korotkevich, G., Sukhov, V., and Sergushichev, A. (2019). Fast gene set enrichment analysis.
1285 BioRxiv 060012.

1286 Krige, D., Needham, L.A., Bawden, L.J., Flores, N., Farmer, H., Miles, L.E.C., Stone, E., Callaghan,
1287 J., Chandler, S., Clark, V.L., et al. (2008). CHR-2797: an antiproliferative aminopeptidase
1288 inhibitor that leads to amino acid deprivation in human leukemic cells. Cancer Res. *68*, 6669–
1289 6679.

1290 Kudo, L.C., Parfenova, L., Ren, G., Vi, N., Hui, M., Ma, Z., Lau, K., Gray, M., Bardag-Gorce, F.,
1291 Wiedau-Pazos, M., et al. (2011). Puromycin-sensitive aminopeptidase (PSA/NPEPPS) impedes
1292 development of neuropathology in hPSA/TAU(P301L) double-transgenic mice. Hum. Mol.
1293 Genet. *20*, 1820–1833.

1294 Kuznetsova, A., Brockhoff, P.B., and Christensen, R.H.B. (2017). lmerTest Package: Tests in
1295 Linear Mixed Effects Models. J. Stat. Softw. *82*, 1–26.

1296 Landrum, M.J., Lee, J.M., Benson, M., Brown, G.R., Chao, C., Chitipiralla, S., Gu, B., Hart, J.,
1297 Hoffman, D., Jang, W., et al. (2018). ClinVar: improving access to variant interpretations and
1298 supporting evidence. Nucleic Acids Res. *46*, D1062–D1067.

1299 Laver, T.W., Franco, E.D., Johnson, M.B., Patel, K., Ellard, S., Weedon, M.N., Flanagan, S.E., and
1300 Wakeling, M.N. (2019). SavvyCNV: genome-wide CNV calling from off-target reads. BioRxiv
1301 617605.

1302 Li, H. (2013). Aligning sequence reads, clone sequences and assembly contigs with BWA-MEM.
1303 ArXiv13033997 Q-Bio.

1304 Li, H., Handsaker, B., Wysoker, A., Fennell, T., Ruan, J., Homer, N., Marth, G., Abecasis, G., and
1305 Durbin, R. (2009). The Sequence Alignment/Map format and SAMtools. Bioinformatics *25*,
1306 2078–2079.

1307 Liberzon, A., Subramanian, A., Pinchback, R., Thorvaldsdóttir, H., Tamayo, P., and Mesirov, J.P.
1308 (2011). Molecular signatures database (MSigDB) 3.0. Bioinformatics *27*, 1739–1740.

1309 Lim, Y.W., Chen-Harris, H., Mayba, O., Lianoglou, S., Wuster, A., Bhangale, T., Khan, Z.,
1310 Mariathasan, S., Daemen, A., Reeder, J., et al. (2018). Germline genetic polymorphisms
1311 influence tumor gene expression and immune cell infiltration. Proc. Natl. Acad. Sci. *115*,
1312 E11701–E11710.

1313 Liston, D.R., and Davis, M. (2017). Clinically Relevant Concentrations of Anticancer Drugs: A
1314 Guide for Nonclinical Studies. Clin. Cancer Res. Off. J. Am. Assoc. Cancer Res. *23*, 3489–3498.

1315 Love, M.I., Huber, W., and Anders, S. (2014). Moderated estimation of fold change and
1316 dispersion for RNA-seq data with DESeq2. Genome Biol. *15*, 550.

1317 Löwenberg, B., Morgan, G., Ossenkoppele, G.J., Burnett, A.K., Zachée, P., Dührsen, U., Dierickx,
1318 D., Müller-Tidow, C., Sonneveld, P., Krug, U., et al. (2010). Phase I/II clinical study of Tosedostat,
1319 an inhibitor of aminopeptidases, in patients with acute myeloid leukemia and myelodysplasia. J.
1320 Clin. Oncol. Off. J. Am. Soc. Clin. Oncol. *28*, 4333–4338.

1321 Mawad, R., Becker, P.S., Hendrie, P., Scott, B., Wood, B.L., Dean, C., Sandhu, V., Deeg, H.J.,
1322 Walter, R., Wang, L., et al. (2016). Phase II study of tosedostat with cytarabine or decitabine in
1323 newly diagnosed older patients with acute myeloid leukaemia or high-risk MDS. Br. J. Haematol.
1324 *172*, 238–245.

1325 McDonald, E.R., de Weck, A., Schlabach, M.R., Billy, E., Mavrakis, K.J., Hoffman, G.R., Belur, D.,
1326 Castelletti, D., Frias, E., Gampa, K., et al. (2017). Project DRIVE: A Compendium of Cancer
1327 Dependencies and Synthetic Lethal Relationships Uncovered by Large-Scale, Deep RNAi
1328 Screening. Cell *170*, 577-592.e10.

1329 Menzies, F.M., Hourez, R., Imarisio, S., Raspe, M., Sadiq, O., Chandraratna, D., O'Kane, C., Rock,
1330 K.L., Reits, E., Goldberg, A.L., et al. (2010). Puromycin-sensitive aminopeptidase protects against
1331 aggregation-prone proteins via autophagy. Hum. Mol. Genet. *19*, 4573–4586.

1332 Mills, R.E., Pittard, W.S., Mullaney, J.M., Farooq, U., Creasy, T.H., Mahurkar, A.A., Kemeza, D.M.,
1333 Strassler, D.S., Ponting, C.P., Webber, C., et al. (2011). Natural genetic variation caused by small
1334 insertions and deletions in the human genome. Genome Res. *21*, 830–839.

1335 Mullenders, J., de Jongh, E., Brousali, A., Roosen, M., Blom, J.P.A., Begthel, H., Korving, J.,
1336 Jonges, T., Kranenburg, O., Meijer, R., et al. (2019). Mouse and human urothelial cancer
1337 organoids: A tool for bladder cancer research. Proc. Natl. Acad. Sci. U. S. A. *116*, 4567–4574.

1338 Nadal, R., and Bellmunt, J. (2019). Management of metastatic bladder cancer. Cancer Treat.
1339 Rev. *76*, 10–21.

1340 Nemkov, T., D'Alessandro, A., and Hansen, K.C. (2015). Three-minute method for amino acid
1341 analysis by UHPLC and high-resolution quadrupole orbitrap mass spectrometry. Amino Acids *47*,
1342 2345–2357.

1343 Nemkov, T., Reisz, J.A., Gehrke, S., Hansen, K.C., and D'Alessandro, A. (2019). High-Throughput
1344 Metabolomics: Isocratic and Gradient Mass Spectrometry-Based Methods. Methods Mol. Biol.
1345 Clifton NJ *1978*, 13–26.

1346 Okonechnikov, K., Conesa, A., and García-Alcalde, F. (2016). Qualimap 2: advanced multi-
1347 sample quality control for high-throughput sequencing data. Bioinforma. Oxf. Engl. *32*, 292–
1348 294.

1349 Olivieri, M., Cho, T., Álvarez-Quilón, A., Li, K., Schellenberg, M.J., Zimmermann, M., Hustedt, N.,
1350 Rossi, S.E., Adam, S., Melo, H., et al. (2020). A Genetic Map of the Response to DNA Damage in
1351 Human Cells. Cell *182*, 481-496.e21.

1352 Osada, T., Ikegami, S., Takiguchi-Hayashi, K., Yamazaki, Y., Katoh-Fukui, Y., Higashinakagawa, T.,
1353 Sakaki, Y., and Takeuchi, T. (1999). Increased anxiety and impaired pain response in puromycin-
1354 sensitive aminopeptidase gene-deficient mice obtained by a mouse gene-trap method. J.
1355 Neurosci. Off. J. Soc. Neurosci. *19*, 6068–6078.

1356 Parker, S.J., Rost, H., Rosenberger, G., Collins, B.C., Malmström, L., Amodei, D., Venkatraman,
1357 V., Raedschelders, K., Van Eyk, J.E., and Aebersold, R. (2015). Identification of a Set of
1358 Conserved Eukaryotic Internal Retention Time Standards for Data-independent Acquisition
1359 Mass Spectrometry. Mol. Cell. Proteomics MCP *14*, 2800–2813.

1360 Parker, S.J., Venkatraman, V., and Van Eyk, J.E. (2016). Effect of peptide assay library size and
1361 composition in targeted data-independent acquisition-MS analyses. Proteomics *16*, 2221–2237.

1362 Patel, V.G., Oh, W.K., and Galsky, M.D. (2020). Treatment of muscle-invasive and advanced
1363 bladder cancer in 2020. CA. Cancer J. Clin.

1364 Planells-Cases, R., Lutter, D., Guyader, C., Gerhards, N.M., Ullrich, F., Elger, D.A.,
1365 Kucukosmanoglu, A., Xu, G., Voss, F.K., Reincke, S.M., et al. (2015a). Subunit composition of
1366 VRAC channels determines substrate specificity and cellular resistance to Pt-based anti-cancer
1367 drugs. EMBO J. *34*, 2993–3008.

1368 Planells-Cases, R., Lutter, D., Guyader, C., Gerhards, N.M., Ullrich, F., Elger, D.A.,
1369 Kucukosmanoglu, A., Xu, G., Voss, F.K., Reincke, S.M., et al. (2015b). Subunit composition of
1370 VRAC channels determines substrate specificity and cellular resistance to Pt-based anti-cancer
1371 drugs. EMBO J. *34*, 2993–3008.

1372 Reid, A.H.M., Protheroe, A., Attard, G., Hayward, N., Vidal, L., Spicer, J., Shaw, H.M., Bone, E.A.,
1373 Carter, J., Hooftman, L., et al. (2009). A First-in-Man Phase I and Pharmacokinetic Study on CHR-
1374 2797 (Tosedostat), an Inhibitor of M1 Aminopeptidases, in Patients with Advanced Solid
1375 Tumors. Clin. Cancer Res. *15*, 4978–4985.

1376 Ritchie, M.E., Phipson, B., Wu, D., Hu, Y., Law, C.W., Shi, W., and Smyth, G.K. (2015). limma
1377 powers differential expression analyses for RNA-sequencing and microarray studies. Nucleic
1378 Acids Res. *43*, e47.

1379 Robertson, A.G., Kim, J., Al-Ahmadie, H., Bellmunt, J., Guo, G., Cherniack, A.D., Hinoue, T., Laird,
1380 P.W., Hoadley, K.A., Akbani, R., et al. (2017). Comprehensive Molecular Characterization of
1381 Muscle-Invasive Bladder Cancer. Cell *171*, 540-556.e25.

1382 Robinson, A.E., Binek, A., Venkatraman, V., Searle, B.C., Holewinski, R.J., Rosenberger, G.,
1383 Parker, S.J., Basisty, N., Xie, X., Lund, P.J., et al. (2020). Lysine and Arginine Protein Post-
1384 translational Modifications by Enhanced DIA Libraries: Quantification in Murine Liver Disease. J.
1385 Proteome Res. *19*, 4163–4178.

1386 Robinson, M.D., McCarthy, D.J., and Smyth, G.K. (2010). edgeR: a Bioconductor package for
1387 differential expression analysis of digital gene expression data. Bioinforma. Oxf. Engl. *26*, 139–
1388 140.

1389 Röst, H.L., Rosenberger, G., Navarro, P., Gillet, L., Miladinović, S.M., Schubert, O.T., Wolski, W.,
1390 Collins, B.C., Malmström, J., Malmström, L., et al. (2014). OpenSWATH enables automated,
1391 targeted analysis of data-independent acquisition MS data. Nat. Biotechnol. *32*, 219–223.

1392 Röst, H.L., Liu, Y., D'Agostino, G., Zanella, M., Navarro, P., Rosenberger, G., Collins, B.C., Gillet,
1393 L., Testa, G., Malmström, L., et al. (2016). TRIC: an automated alignment strategy for
1394 reproducible protein quantification in targeted proteomics. Nat. Methods *13*, 777–783.

1395 Rottenberg, S., Disler, C., and Perego, P. (2021). The rediscovery of platinum-based cancer
1396 therapy. Nat. Rev. Cancer *21*, 37–50.

1397 Saric, T., Graef, C.I., and Goldberg, A.L. (2004). Pathway for degradation of peptides generated
1398 by proteasomes: a key role for thimet oligopeptidase and other metallopeptidases. J. Biol.
1399 Chem. *279*, 46723–46732.

1400 Schönlein, C., Löffler, J., and Huber, G. (1994). Purification and characterization of a novel
1401 metalloprotease from human brain with the ability to cleave substrates derived from the N-
1402 terminus of beta-amyloid protein. Biochem. Biophys. Res. Commun. *201*, 45–53.

1403 Sergushichev, A.A. (2016). An algorithm for fast preranked gene set enrichment analysis using
1404 cumulative statistic calculation. BioRxiv 060012.

1405 Sherry, S.T., Ward, M.H., Kholodov, M., Baker, J., Phan, L., Smigielski, E.M., and Sirotkin, K.
1406 (2001). dbSNP: the NCBI database of genetic variation. Nucleic Acids Res. *29*, 308–311.

1407 Sørensen, B.H., Thorsteinsdottir, U.A., and Lambert, I.H. (2014). Acquired cisplatin resistance in
1408 human ovarian A2780 cancer cells correlates with shift in taurine homeostasis and ability to
1409 volume regulate. Am. J. Physiol.-Cell Physiol. *307*, C1071–C1080.

1410 Sørensen, B.H., Nielsen, D., Thorsteinsdottir, U.A., Hoffmann, E.K., and Lambert, I.H. (2016a).
1411 Downregulation of LRRC8A protects human ovarian and alveolar carcinoma cells against
1412 Cisplatin-induced expression of p53, MDM2, p21Waf1/Cip1, and Caspase-9/-3 activation. Am. J.
1413 Physiol.-Cell Physiol. *310*, C857–C873.

1414 Sørensen, B.H., Dam, C.S., Stürup, S., and Lambert, I.H. (2016b). Dual role of LRRC8A-containing
1415 transporters on cisplatin resistance in human ovarian cancer cells. J. Inorg. Biochem. *160*, 287–
1416 295.

1417 Syeda, R., Qiu, Z., Dubin, A.E., Murthy, S.E., Florendo, M.N., Mason, D.E., Mathur, J., Cahalan,
1418 S.M., Peters, E.C., Montal, M., et al. (2016). LRRC8 Proteins Form Volume-Regulated Anion
1419 Channels that Sense Ionic Strength. Cell *164*, 499–511.

1420 Teleman, J., Röst, H.L., Rosenberger, G., Schmitt, U., Malmström, L., Malmström, J., and
1421 Levander, F. (2015). DIANA--algorithmic improvements for analysis of data-independent
1422 acquisition MS data. Bioinforma. Oxf. Engl. *31*, 555–562.

1423 Towne, C.F., York, I.A., Neijssen, J., Karow, M.L., Murphy, A.J., Valenzuela, D.M., Yancopoulos,
1424 G.D., Neefjes, J.J., and Rock, K.L. (2008). Puromycin-Sensitive Aminopeptidase Limits MHC Class
1425 I Presentation in Dendritic Cells but Does Not Affect CD8 T Cell Responses during Viral
1426 Infections. J. Immunol. *180*, 1704–1712.

1427 Tsherniak, A., Vazquez, F., Montgomery, P.G., Weir, B.A., Kryukov, G., Cowley, G.S., Gill, S.,
1428 Harrington, W.F., Pantel, S., Krill-Burger, J.M., et al. (2017). Defining a Cancer Dependency Map.
1429 Cell *170*, 564-576.e16.

1430 Uhlen, M., Zhang, C., Lee, S., Sjöstedt, E., Fagerberg, L., Bidkhori, G., Benfeitas, R., Arif, M., Liu,
1431 Z., Edfors, F., et al. (2017). A pathology atlas of the human cancer transcriptome. Science *357*.

1432 Vale, C.L. (2005). Neoadjuvant Chemotherapy in Invasive Bladder Cancer: Update of a
1433 Systematic Review and Meta-Analysis of Individual Patient Data: Advanced Bladder Cancer
1434 (ABC) Meta-analysis Collaboration. Eur. Urol. *48*, 202–206.

1435 Vallo, S., Michaelis, M., Rothweiler, F., Bartsch, G., Gust, K.M., Limbart, D.M., Rödel, F., Wezel,
1436 F., Haferkamp, A., and Cinatl, J. (2015). Drug-Resistant Urothelial Cancer Cell Lines Display
1437 Diverse Sensitivity Profiles to Potential Second-Line Therapeutics. Transl. Oncol. *8*, 210–216.

1438 Vallo, S., Köpp, R., Michaelis, M., Rothweiler, F., Bartsch, G., Brandt, M.P., Gust, K.M., Wezel, F.,
1439 Blaheta, R.A., Haferkamp, A., et al. (2017). Resistance to nanoparticle albumin-bound paclitaxel
1440 is mediated by ABCB1 in urothelial cancer cells. Oncol. Lett. *13*, 4085–4092.

1441 Voss, F.K., Ullrich, F., Münch, J., Lazarow, K., Lutter, D., Mah, N., Andrade-Navarro, M.A., von
1442 Kries, J.P., Stauber, T., and Jentsch, T.J. (2014). Identification of LRRC8 heteromers as an
1443 essential component of the volume-regulated anion channel VRAC. Science *344*, 634–638.

1444 Wang, K., Li, M., and Hakonarson, H. (2010). ANNOVAR: functional annotation of genetic
1445 variants from high-throughput sequencing data. Nucleic Acids Res. *38*, e164–e164.

1446 Wickham, H. (2009). Ggplot2: elegant graphics for data analysis (New York: Springer).

Winter, J., Breinig, M., Heigwer, F., Brügemann, D., Leible, S., Pelz, O., Zhan, T., and Boutros, M. (2016). caRpools: an R package for exploratory data analysis and documentation of pooled CRISPR/Cas9 screens. Bioinforma. Oxf. Engl. *32*, 632–634.

Witjes, J.A., Bruins, H.M., Cathomas, R., Compérat, E.M., Cowan, N.C., Gakis, G., Hernández, V., Linares Espinós, E., Lorch, A., Neuzillet, Y., et al. (2020). European Association of Urology Guidelines on Muscle-invasive and Metastatic Bladder Cancer: Summary of the 2020 Guidelines. Eur. Urol.

Yanagi, K., Tanaka, T., Kato, K., Sadik, G., Morihara, T., Kudo, T., and Takeda, M. (2009). Involvement of puromycin-sensitive aminopeptidase in proteolysis of tau protein in cultured cells, and attenuated proteolysis of frontotemporal dementia and parkinsonism linked to chromosome 17 (FTDP-17) mutant tau. Psychogeriatrics *9*, 157–166.

Yu, G., Wang, L.-G., Han, Y., and He, Q.-Y. (2012). clusterProfiler: an R Package for Comparing Biological Themes Among Gene Clusters. OMICS J. Integr. Biol. *16*, 284–287.

Zhou, Y., Zhou, B., Pache, L., Chang, M., Khodabakhshi, A.H., Tanaseichuk, O., Benner, C., and Chanda, S.K. (2019). Metascape provides a biologist-oriented resource for the analysis of systems-level datasets. Nat. Commun. *10*, 1523.

(2018). Picard toolkit (Broad Institute).

Figure Legends

Figure 1. Project overview and synthetic lethal screen results. (**A**) Human bladder cancer cell lines were made resistant to cisplatin, gemcitabine, or gemcitabine plus cisplatin through dose escalation. All cell lines were profiled using -omic technologies. The gemcitabine plus cisplatin resistant cells were subjected to a pooled CRISPR screen to identify synthetic lethal gene-to-drug relationships. (**B**) Aggregate gene set enrichment results for the synthetic lethal screen results across all cell lines reveal DNA damage response and repair pathways. Each tick mark represents a gene in the associated pathway. The bars are normalized enrichment scores (NES) with the FDR corrected p-values reported in the bars. (**C**) When results from all cell lines were evaluated individually, a total of 46 commonly synthetic lethal genes were identified; all counts are reported in **Figure S2**. (**D**) The percentage change in the aggregate of the sgRNAs targeting the 46 commonly synthetic lethal genes are reported across saline (PBS) or gemcitabine plus cisplatin treatment arms of the CRISPR screen.

Figure 2. NPEPPS is identified as a commonly upregulated and synthetic lethal hit. (**A**) Differential gene expression of the 46 common synthetic lethal genes as measured by RNAseq across all cell lines, comparing the treatment resistant derivative (Gem-, Cis-, GemCis-resistant) to the associated parental cell line. Asterisks indicate a statistically significant result (moderated t-test, *FDR < 0.05). The top bar plot is the aggregate count of significant results across all 15 comparisons. Genes are ranked by the count of statistically significant upregulated hits. (**B**) RNAseq (compared to parentals; *FDR < 0.05), (**C**) mass spectrometry proteomics (compared to parentals, *FDR < 0.25), and (**D**) CRISPR screen results (*FDR < 0.05) for NPEPPS. (**E**) Representative immunoblots and densitometry quantification for independent triplicates (mean ± SEM) for NPEPPS in all cell lines (*FDR < 0.05).

Figure 3. Genetic and pharmacological inhibition of NPEPPS resensitizes GemCis-resistant cells. (**A**) NPEPPS was found to be synthetic lethal with cisplatin in a CRISPR screen for 27 genotoxic agents in RPE1 cells by (Olivieri et al., 2020). (**B**) Immunoblot for NPEPPS across several control and shRNAs targeting NPEPPS. (**C, D**)KU1919-GemCis cells with knockdown of NPEPPS treated with increasing doses of cisplatin or gemcitabine. A total of 3 technical replicates per dose (mean ± SEM). Independent experiments are reported in **Figure S5**. (**E**) NPEPPS mRNA is upregulated in response to cisplatin treatment in a dose dependent manner if both KU1919 parental and GemCis-resistant cells. Independent triplicate experiments are shown (mean ± SEM) (t-test compared to 0μM; *p < 0.05, **p < 0.05). (**F**) Pharmacologic targeting of NPEPPS with tosedostat in GemCis-resistant cells treated with cisplatin, gemcitabine, and gemcitabine plus cisplatin treatment. A total of 3 technical replicates per dose are shown (mean ± SEM). Independent experiments are reported in **Figure S6**.

Figure 4. NPEPPS interacts with volume regulated anion channel (VRAC) subunits LRRC8A and LRRC8D to mediate cisplatin response. (**A**) NPEPPS is found to interact with all VRAC subunits, LRRC8A-E, using the BioPlex interactome (Huttlin et al., 2020). (**B, C**) Knockout of LRRC8A and LRRC8D through the CRISPR screen resulted in increased cell growth upon gemcitabine plus cisplatin treatment in GemCis-resistant cell lines (moderated t-test; *FDR < 0.05). (**D**) Genes ranked based on $\log_2$ fold change from the synthetic lethal CRISPR screens across all cell lines. LRRC8A-E and the 46 common synthetic lethal genes are labeled. (**E, F**) LRRC8A and LRRC8D gene expression measured by RNAseq (compared to parentals; *FDR < 0.05). (**G**) Volcano plot of metabolites measured from KU1919-GemCis cells with or without NPEPPS knockdown (shN39). Time and treatment (cisplatin 10μM) were covariates in the linear model to calculate differential expression using a moderated t-test;

horizontal grey line is -$\log_{10}$(FDR = 0.05). (**H**)Taurine abundance measured in KU1919-GemCis cells with non-targeting shRNA controls or shRNA targeting NPEPPS. Cells were also measured at 48 hours with cisplatin treatment or PBS, vehicle control. (**I**) Intracelullar cisplatin levels were measured after 4 hours of treatment at 10μM cisplatin using CyTOF, with the number of cells analyzed as indicated. The median Pt 195 measurement for the KU1919-parental line = 158, for the KU1919-GemCis line = 44.5, and for the KU1919-GemCis- shN39 line = 77. (**J**) Immunoblot of LRRC8A, LRRC8D, and γH2AX in KU1919-GemCis-shCtrl1 and KU1919-GemCis-shN39 cells treated with PBS or 10μM cisplatin for 38 hours.

Figure 5. Genetic and pharmacological inhibition of NPEPPS resensitizes *in vivo* and *ex vivo* models of bladder cancer to cisplatin-based chemotherapy. (**A**) Tumor volume of KU1919-GemCis xenografts measured over time and across 4 treatment groups considering non-targeting shRNA controls (shCtrl1), shRNA targeting NPEPPS (shN39), PBS vehicle control (PBS), or gemcitabine plus cisplatin treatment (GemCis). (**B**) Survival analysis of xenograft models with a defined endpoint of a tumor volume > 2cm^3. Logrank test was applied to test significance. (**C, D, E**) Patient tumor-derived organoids were derived from patient tumors that did not respond to gemcitabine plus cisplatin chemotherapy. Organoids were treated for 6 days, allowed to recover for 10 days, then reseeded at different ratios depending on overall growth, then allowed to grow for an additional 6 days. Cell viability was quantified in triplicate after reseeding (t-test; * $p<0.05$, ** $p<e^{-3}$, *** $p<e^{-5}$). (**F**) Survival analysis of muscle-invasive bladder cancer in the TCGA stratified based on copy number amplification, gain or overexpression of LRRC8A or LRRC8D. Patients all had a record of cisplatin-based chemotherapy treatment. (**G**) Survival analysis for patients stratified by LRRC8A or LRRC8D as in (**F**), but did not have any record of cisplatin-based treatments.

Figure 6. Proposed model of NPEPPS-mediated cisplatin resistance. Normal functioning cells will import cisplatin through the volume regulated anion channels (VRAC), with LRRC8A and LRRC8D being the primary subunits. A mechanism of cisplatin resistance is to have inherently down-regulated VRACs. We propose that NPEPPS interacts with LRRC8A or LRRC8D directly to decrease VRAC activity, which prevents export of taurine and import of cisplatin, hence driving cisplatin resistance.

Figure S1. Dose response for all cell line derivatives. Parental, cisplatin-resistant, gemcitabine-resistant, and gemcitabine plus cisplatin (GemCis)-resistant cells for each of the five bladder cancer cell lines were treated with increasing doses of cisplatin or gemcitabine. Dose response curves were calculated. The resistant derivative lines were more resistant to the associated drug. Data represent a single experiment with each condition measured in technical triplicate wells (mean ± SEM).

Figure S2. Venn diagram of synthetic lethal genes. The number of genes that were statistically significantly synthetic lethal (FDR < 0.05) are reported.

Figure S3. Resistance mechanisms of gemcitabine. (**A**) Gemcitabine is processed through several mechanisms to have its downstream treatment impact, leading to chain termination, impaired DNA repair, and finally apoptosis. Deoxycitadine kinase (DCK) and ribonucleotide reductase subunit M1 (RRM1) are known mechanisms of gemcitabine resistance. (**B**) Transcript and protein expression are reported for both genes (ND = not detected; *FDR < 0.01). In addition, copy number results are shown for all cell lines.

Figure S4. Synthetic lethal screen comparison. (**A**) The results from the CRISPR screen reported in this study were correlated with the synthetic lethal screen results for 27 genotoxic agents from (Olivieri et al., 2020). The screen results from the five cell lines reported here are highlighted by the black box and were highly correlated. The drug that was most correlated with our screen results was cisplatin. (**B**) The synthetic lethal results for the top 46 hits reported here are shown including results from the Olivieri et al dataset. 42 genes are reported as four genes did not map to the Olivieri et al dataset. The synthetic lethal scores were z-score normalized for display purposes and show that the 42 genes were also synthetic lethal in the three cisplatin screens, but not in the gemcitabine screen.

Figure S5. shRNA and siRNA targeting NPEPPS resensitizes to cisplatin and gemcitabine plus cisplatin. (**A**) Dose response for shRNA targeting NPEPPS (shN38 = TRCN0000073838; shN39 = TRCN0000073839; shN40 = TRCN0000073840) or non-targeting controls (shCtrl1 = MISSION pLKO.1-puro Non-Mammalian shRNA Control; shCtrl2 = MISSION pLKO.1-puro Non-Target shRNA Control). Cells were treated with cisplatin or gemcitabine separately. Data for KU1919 shown from two independent experiments with 3 technical replicates per dose (mean ± SEM). Data from 253J represent a single experiment with 3 technical replicate wells per dose (mean ± SEM). (**B**) Immunoblot analysis of NPEPPS protein across the different shRNAs and cell lines. (**C**) Cell confluency was measured using Incucyte Zoom across untransfected cells, siRNA controls (siCtrl), and siRNA transfected cells targeting NPEPPS. Cells were treated with PBS or gemcitabine plus cisplatin (GemCis) at the resistant doses for each cell line (**Table S1**). Data shown represent a single experiment with 3 technical replicates (mean ± SEM) per timepoint represented.

Figure S6. Response to tosedostat in combination with gemcitabine, cisplatin, or gemcitabine plus cisplatin. Dose response curves for serial increased doses of tosedostat at 120 hours at the associated resistant doses of gemcitabine or cisplatin for each cell line (**Table S1**). Data represent triplicate wells per dose, per experiment (mean ± SEM).

Figure S7. LRRC8D gene expression and copy number alterations. Gene expression shows that LRRC8D is not detected in the TCCSUP-Cis and TCCSUP-GemCis cell lines. This result is supported by a focal copy number deletion detected using WES data that is specific to the TCCSUP-Cis and TCCSUP-GemCis cell lines (*FDR < 0.01).

Figure S8. Intracellular cisplatin measured using CyTOF. KU1919-Parental, KU1919-GemCis and KU1919-GemCis-shN39 cells were treated with PBS vehicle (0μM) or 10μM cisplatin for 4 hours and then intracellular cisplatin was measured using cytometry by time of flight (CyTOF). Results from (**A**) replicate 1 and (**B**) replicate 2 are shown. (**C**) Immunoblotting for γH2AX, LRRC8A, and LRRC8D were performed in KU1919-GemCis-shCtrl1 or KU1919-GemCis-shN39 cells after 48 hours of treatment with 10μM cisplatin or PBS vehicle control. This is an independent replicate from the immunoblot reported in **Figure 4J**.

Figure S9. Xenograft tumor growth modeling and validation. (**A**) Fixed effects population-level model fit (thick lines) overlaid on top of the observations (grey lines). Longitudinal tumor volumes were divided by the baseline tumor volume and then $\log_2$-transformed before modelling. (**B**) Residuals for the final mixed-effects model (y-axis) coupled with the original observations (x-axis). No systematic trends were detected in model diagnostics, suggesting that the single fitted model successfully captured variation over the treatment arms and individuals. (**C**) Immunoblot on the left is from KU1919-GemCis cells that were injected into mice to

establish tumors. Immunoblot on the right are from tumor samples after mice met the endpoint of the experiment of > $2cm^3$.

Figure S10. Patient tumor-derived organoids generated from muscle-invasive bladder cancer patients treated with platinum-based chemotherapy. (**A**) Clinical time course of muscle-invasive bladder cancer patients from whom patient tumor-derived organoid lines were initiated after radical cystectomy. Patients are not lost to follow-up but censored, at the time of publication. TURBT = transurethral resection of bladder tumor. (**B**) Bright-field images of organoids together with H&E staining of patient tumors and organoids. (**C**) SNaPshot mutation analysis of patient tumors and organoids on hotspot mutations in fibroblast growth factor receptor 3 (*FGFR3*) or telomerase reverse transcriptase (*TERT*). Copy number plot of the entire genome for the primary tumor and organoids from patient 65 demonstrate the genomic similarity of the tumor-derived organoids. Intensity values of each bin are plotted as colored dots, with each chromosome represented by a different color. (**D**) Overall experimental design for treating the organoids with cisplatin, tosedostat, or the combination cisplatin plus tosedostat. Organoids were withdrawn from treatment after 6 days of treatment and reseeded after 16 days of treatment. Cell viability was measured using alamarBlue.

Figure S11. Patient tumor-derived organoids derived from patient 1 and treated with tosedostat and/or cisplatin. (**A**) Organoids were treated for 6 days at the indicated concentrations of drug. Cell viability was quantified using alamarBlue. (**B**) Organoids were then withdrawn from treatment for 10 days and assayed again for cell viability using alamarBlue. (**C**) Organoids were reseeded and allowed to regrow for 6 days and cell viability was tested using alamarBlue. (**D**) Comparison of tosedostat doses over the course of treatment and withdrawal. All comparisons were done in triplicate (t-test; * $p<0.05$, ** $p<e^{-3}$, *** $p<e^{-5}$).

Figure S12. Patient tumor-derived organoids derived from patient 2 and treated with tosedostat and/or cisplatin. (**A**) Organoids were treated for 6 days at the indicated concentrations of drug. Cell viability was quantified using alamarBlue. (**B**) Organoids were then withdrawn from treatment for 10 days and assayed again for cell viability using alamarBlue. (**C**) Organoids were reseeded and allowed to regrow for 6 days and cell viability was tested using alamarBlue. All comparisons were done in triplicate (t-test; * $p<0.05$, ** $p<e^{-3}$, *** $p<e^{-5}$).

Figure S13. Patient tumor-derived organoids derived from patient 3 and treated with tosedostat and/or cisplatin. (**A**) Organoids were treated for 6 days at the indicated concentrations of drug. Cell viability was quantified using alamarBlue. (**B**) Organoids were then withdrawn from treatment for 10 days and assayed again for cell viability using alamarBlue. (**C**) Organoids were reseeded and allowed to regrow for 6 days and cell viability was tested using alamarBlue. All comparisons were done in triplicate (t-test; * $p<0.05$, ** $p<e^{-3}$, *** $p<e^{-5}$).

Tables

Feature	KU1919	T24	TCCSUP	5637	253J
Sex	Male	Female	Female	Male	Female
Stage	T3	Ta	N/A	N/A	T4
Grade	G3	G3	G4	G2	G4
Base47 Subtype	N/A	Basal	Basal	Luminal	Basal
TP53		Y126X	E349X		
HRAS		G12V			

NRAS	Q61R				
PIK3CA			E545K		E545G
TERT					
ARID1A	Y1052X				
KMT2D	T2441Pfs*44			Q2813X	
KDM6A	Q915X				
FAT1		S2682X	D1536N		
KMT2C		R4225X; A3559T			
ERBB2				S310F	
ERBB3		E1219K			
EP300		C1201Y			
FBXW7			S66X		
ASXL2			E330Q		
ATM				H1876Q	
AKT1	E17K				
RYR2		R2401H			
NFE2L2					G81S
RB1			LOSS	Y325X	
E2F3			AMP	AMP	
PPARG				AMP	
CCND1	AMP				
CDKN2A	LOSS				LOSS

Table 1. Clinicopathologic characteristics and genetic drivers for five cell lines.

Figure 1

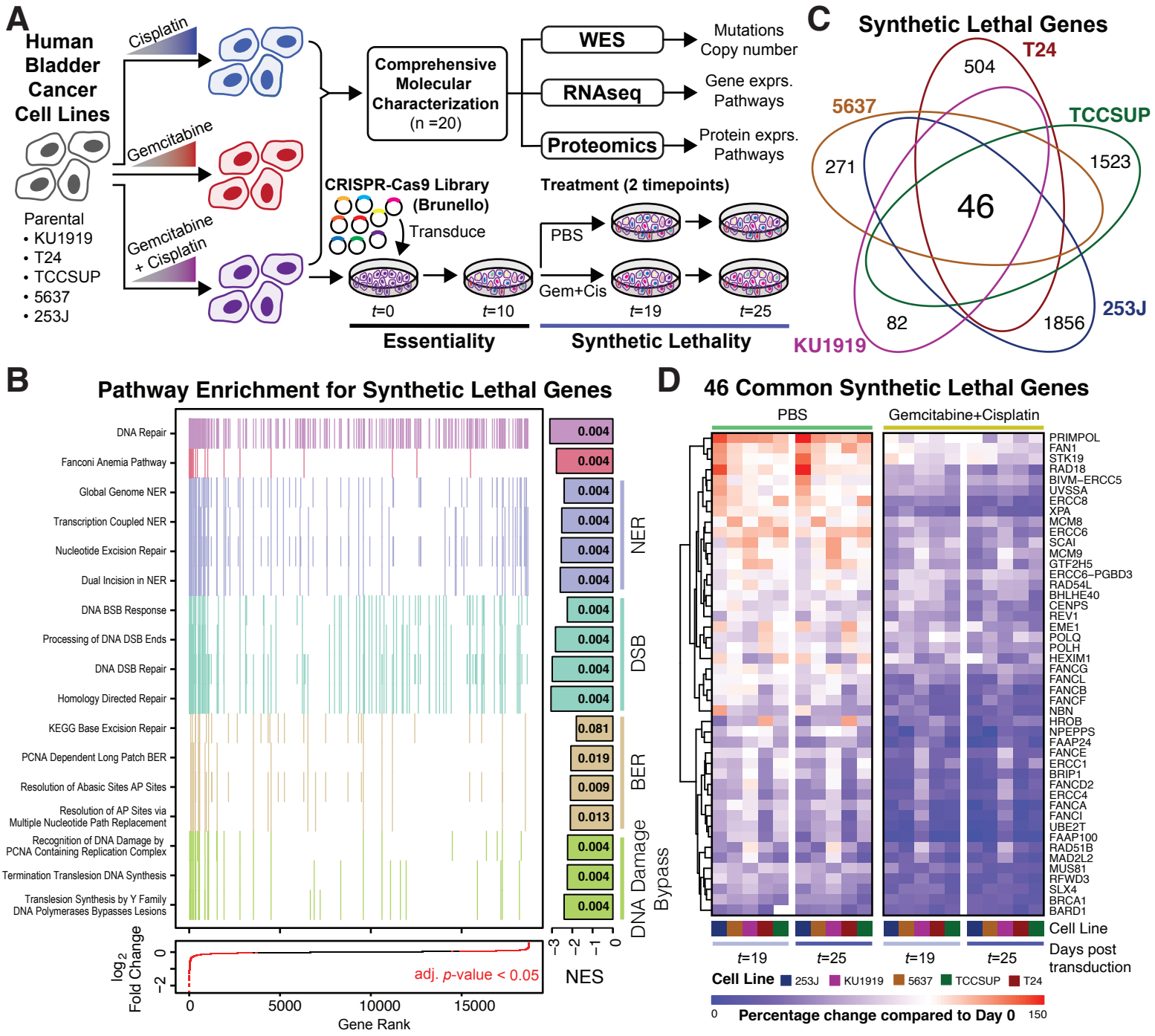

Figure 2

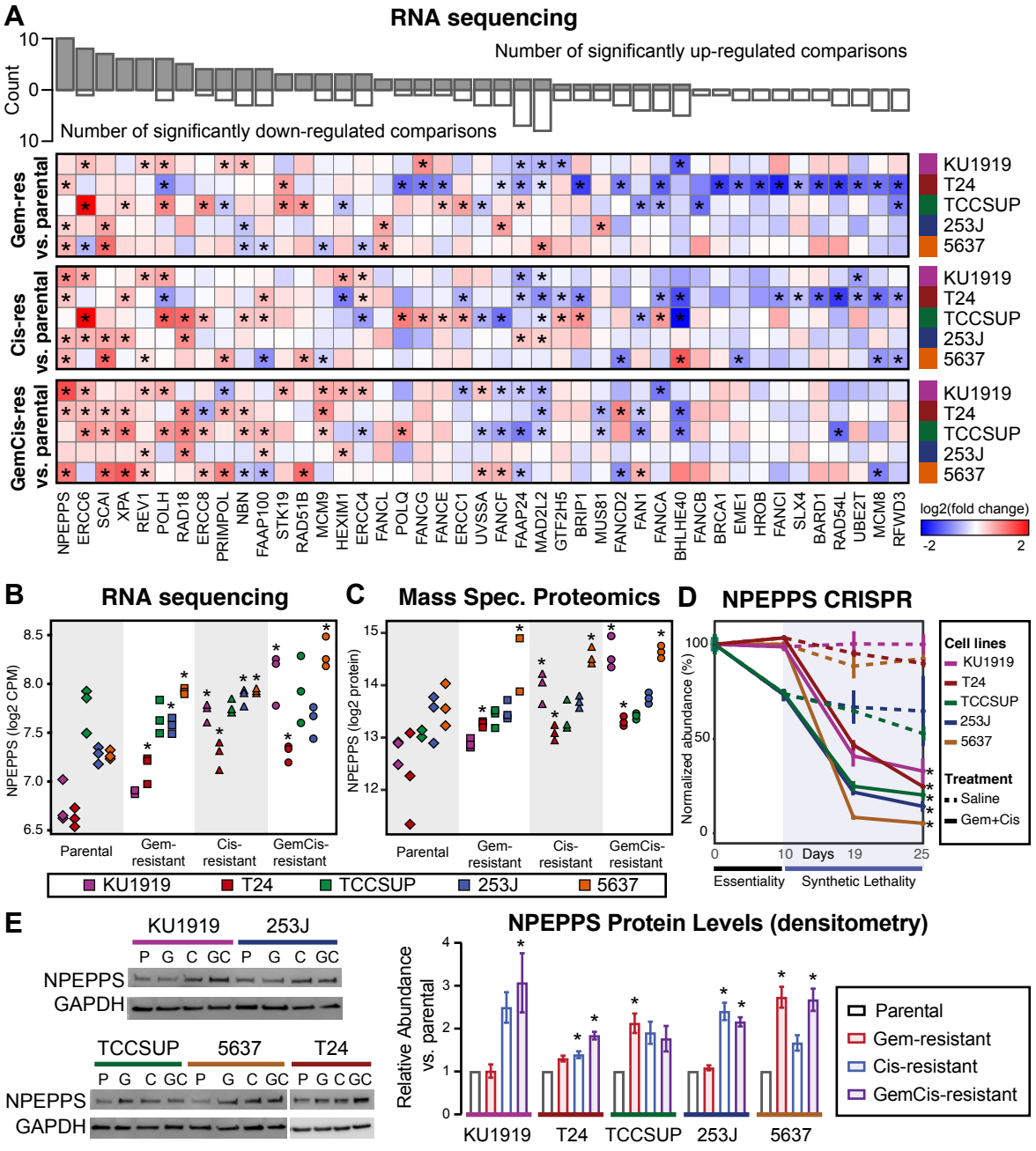

Figure 3

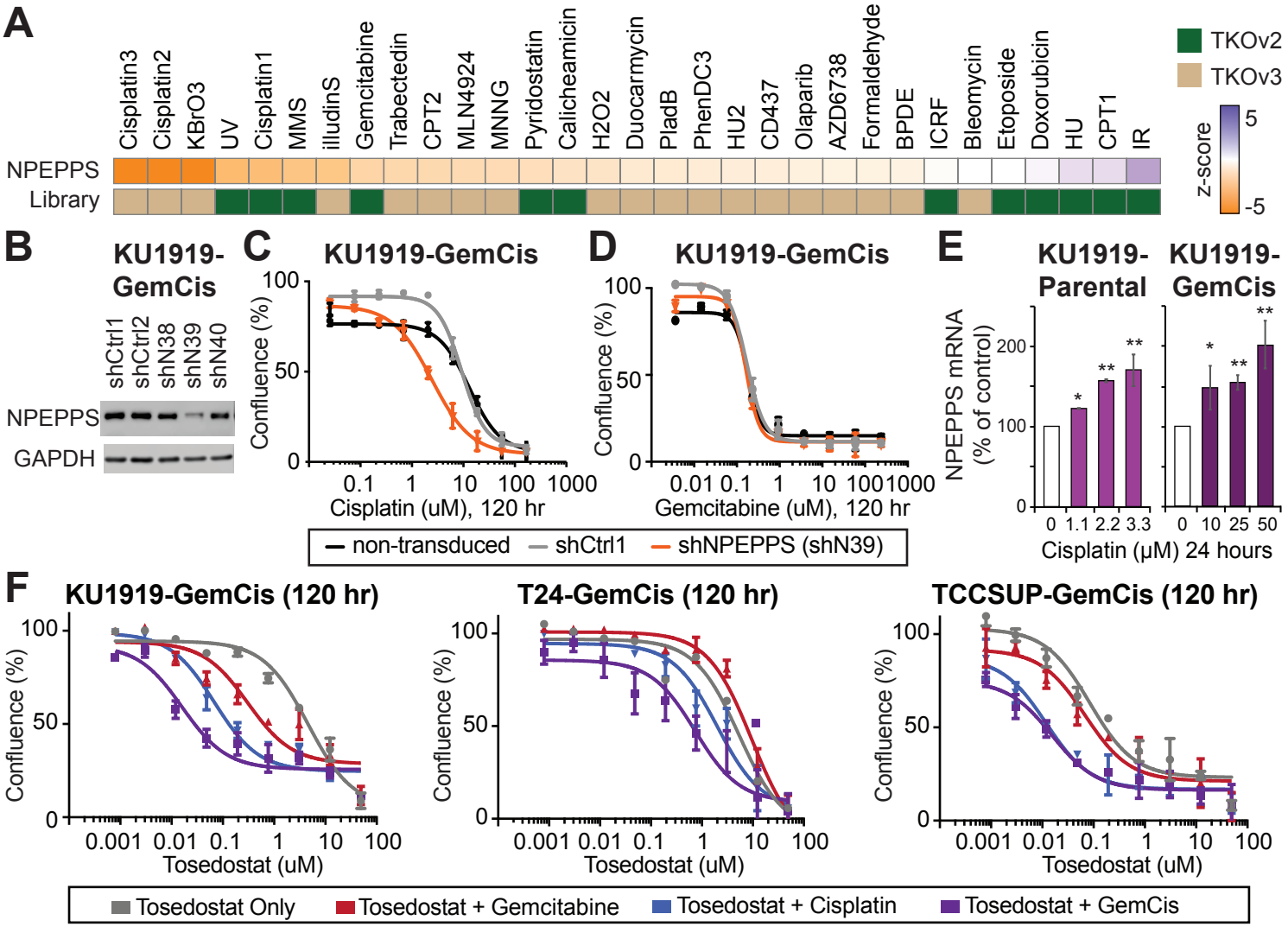

Figure 4

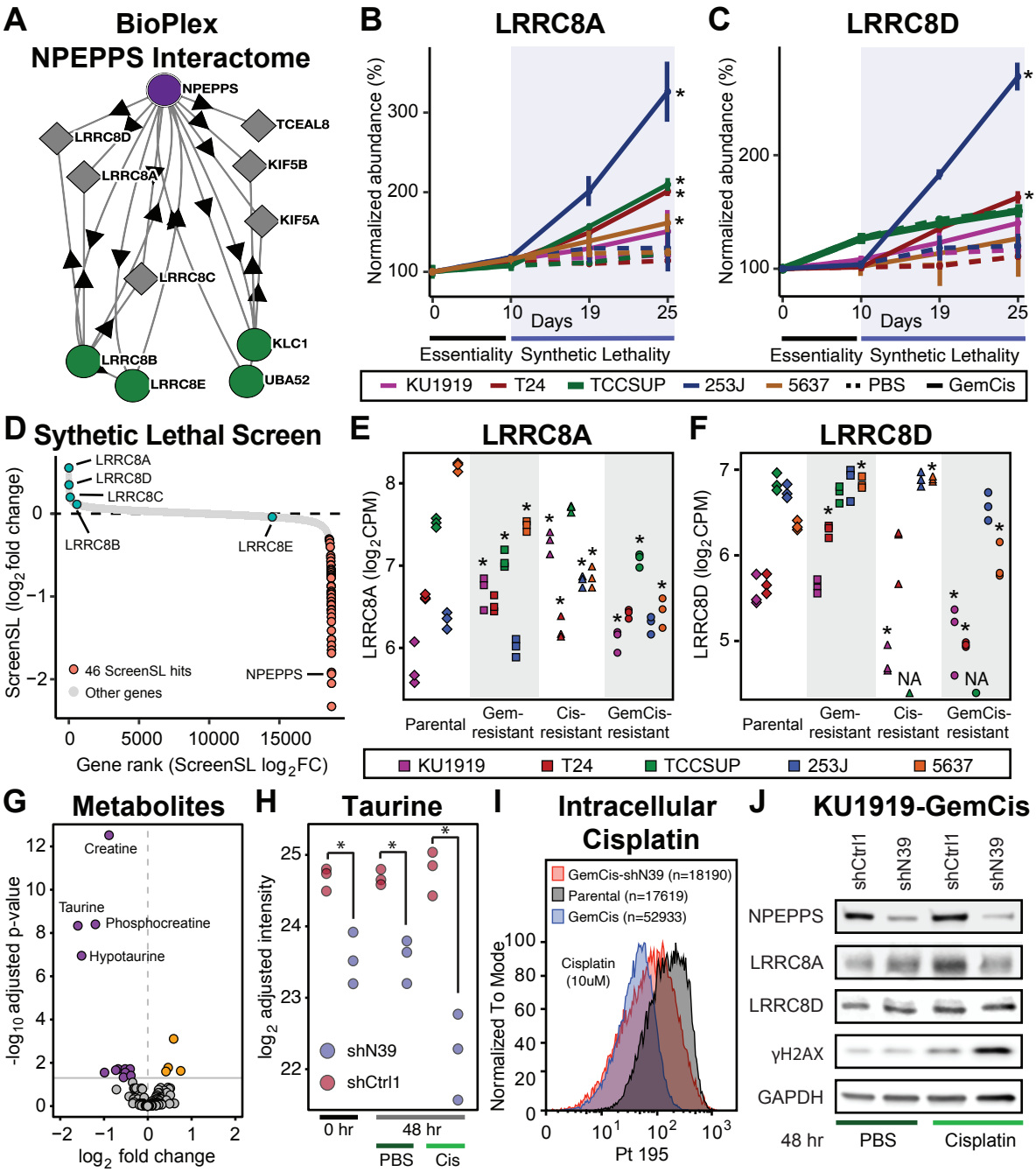

Figure 5

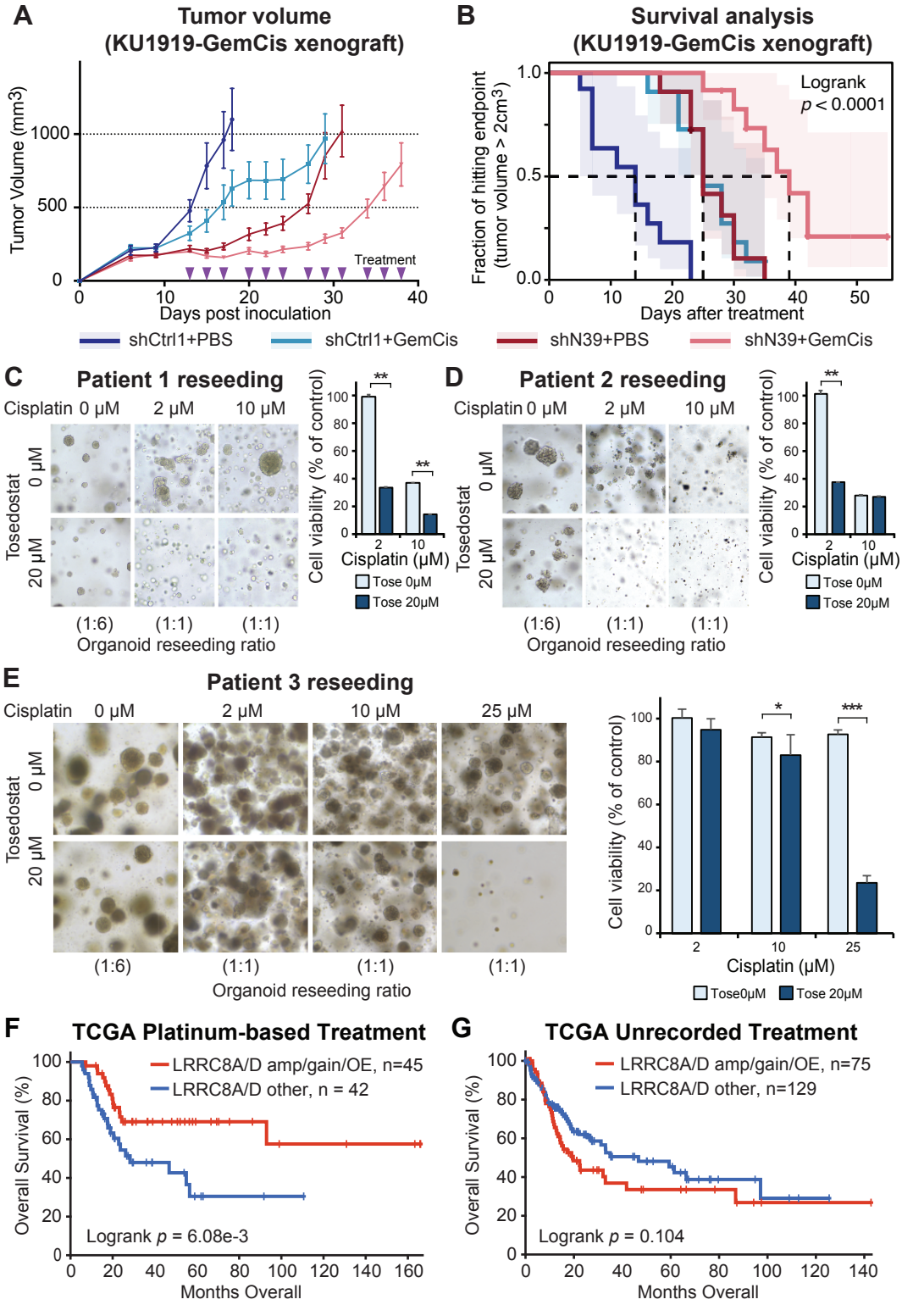

Figure 6